ADDIS ABABA UNIVERSITY
GRADUATE STUDIES PROGRAM
EARTH SCIENCE DEPARTMENT

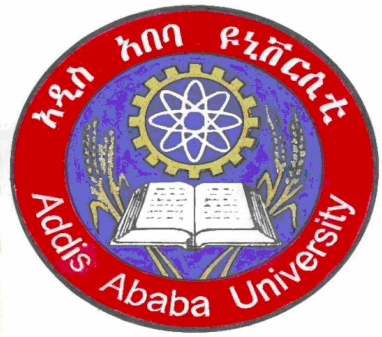

Geophysical Investigations for Groundwater Potential Assessment and Mapping Structures for possible connections between Lakes Langano and Shala, Main Ethiopian Rift

BY: TAGEL ASSEFA

A Thesis submitted to the School of Graduate Studies, Addis Ababa University, in partial fulfillment of the requirements of the Degree Master of Science in Exploration Geophysics.

DECEMBER, 2008

ADDIS ABABA UNIVERSITY

DEPARTMENT OF EARTH SCIENCE

SCHOOL OF GRADUATE STUDIES

Geophysical Investigations for Groundwater Potential Assessment and Mapping Structures for possible connections between Lakes Langano and Shala, Main Ethiopian Rift

BY
Tagel Assefa Dendi
Faculty of science
Department of Earth Sciences

Approved by Board Examiners:

Dr. Balemwal Atnafu

_____

(Chairman, Department Graduate Committee) Signature

Dr.Tigistu Haile

_____

Advisor Signature

Dr. Shimelis Fisseha

_____

Internal examiner Signature

Dr. Getnet Mewa

_____

External examiner Signature

Abstract

A low-lying narrow corridor covers the region between the two major lakes in the Main Ethiopian Rift-Lakes Langano and Shala. Owing to the differences in surface elevation between the two lakes and the fact that the region is affected by tectonism, the presence of possible subsurface rift structures and flow of fluids between the lakes has been postulated.

Geophysical surveys, involving electrical resistivity, gravity and magnetic surveys have been carried out over the corridor to verify the presence of these structures. Three traverses, approximately selected to cross the area have been used for surveys. Nine VES points, 105 gravity and about 181 magnetic data have been collected and analyzed. The results are presented in the form of electrical pseudosections and geoelectricsections and also anomaly plots and modeled sections and interpreted to verify the presence of such features within the corridor.

From the electrical survey data analysis it is seen that corridor between the two lakes is represented by an extensive low resistivity response region which is believed to result from a highly saturated subsurface horizon. The electrical survey has also mapped the presence of structures whose orientation makes them a candidate to act as fluid paths between the lakes. The gravity and magnetic data have been modeled together to depict the lateral and depth variations in density and magnetic susceptibility. These results also show the presence of structures that could act as paths for interchange of fluids between the two lakes.

Acknowledgements

My acknowledgement goes first and for most to my advisor, Dr Tigistu Haile for his proper guidance throughout the study.

I am indebted to the staff of the Geological Survey of Ethiopia especially Dr. Getnet Mewa, Ato Dawit Mamo, Ato Aklilu Haile and Ato Tamirat Fantanye who helped me a lot on data reductions as well as preparing modeled sections and anomaly maps.

I would like to acknowledge Dr. Tilahun Mamo for providing me useful information from the EAGLE project which help me a lot on preparing the modeled sections. Furthermore my acknowledgement also goes to Dr. Tenalem Ayenew for his valuable comments on my work and material supports.

At last but not the least, my deepest gratitude and acknowledgements goes to the MAWARI project and Dire Dawa Education Bureau for providing me the financial support to conduct the research.

TABLE OF CONTENTS

FIGURES AND TABLES

TABLES **Page**

CHAPTER ONE

INTRODUCTION

1.1 GENERAL

The East African Rift System (EARS) is one the geologic wonders of the world, a place where the earth's tectonic forces are presently trying to create new plates by splitting apart old ones. In simple terms, a rift can be thought of as a fracture in the earth's surface that widens over time, or more technically, as an elongate basin bounded by opposed steeply dipping normal faults. Geologists are still debating exactly how rifting comes about, but the process is so well displayed in East Africa that geologists have attached a name to the new plate-to-be; the Nubian Plate makes up most of Africa, while the smaller plate that is pulling away has been named the Somalian Plate (Figure 1.1). These two plates are moving away form each other and also away from the Arabian plate to the north. The point where these three plates meet in the Afar region of Ethiopia forms what is called a triple-junction. However, all the rifting in East Africa is not confined to the Horn of Africa; there is a lot of rifting activity further south as well, extending into Kenya and Tanzania and Great Lakes region of Africa.

The exact mechanism of rift formation is an on-going debate among geologists and geophysicists. One popular model for the EARS assumes that elevated heat flow from the mantle (strictly the asthenosphere) is causing a pair of thermal "bulges" in central Kenya and the Afar region of north-central Ethiopia. These bulges can be easily seen as elevated highlands on any topographic map of the area. As these bulges form, they stretch and fracture the outer brittle crust into a series of normal faults forming the classic horst and graben structure of rift valleys. Most current geological thinking holds that bulges are initiated by mantle plumes under the continent heating the overlying crust and causing it to expand and fracture. Ideally the dominant fractures created occur in a pattern consisting of three fractures or fracture zones radiating from a point with an angular separation of 120 degrees. The point from which the three branches radiate is called a "triple junction" and is well illustrated in the Afar region of Ethiopia (Figure 1.1), where two branches are occupied by the Red Sea and Gulf of Aden, and the third rift branch runs to the south through Ethiopia.

The Ethiopian rift system which is part of the East African Rift System may be subdivided into three main sectors. These are the Southwestern Rift zone, the Main Ethiopian Rift and Afar depression.

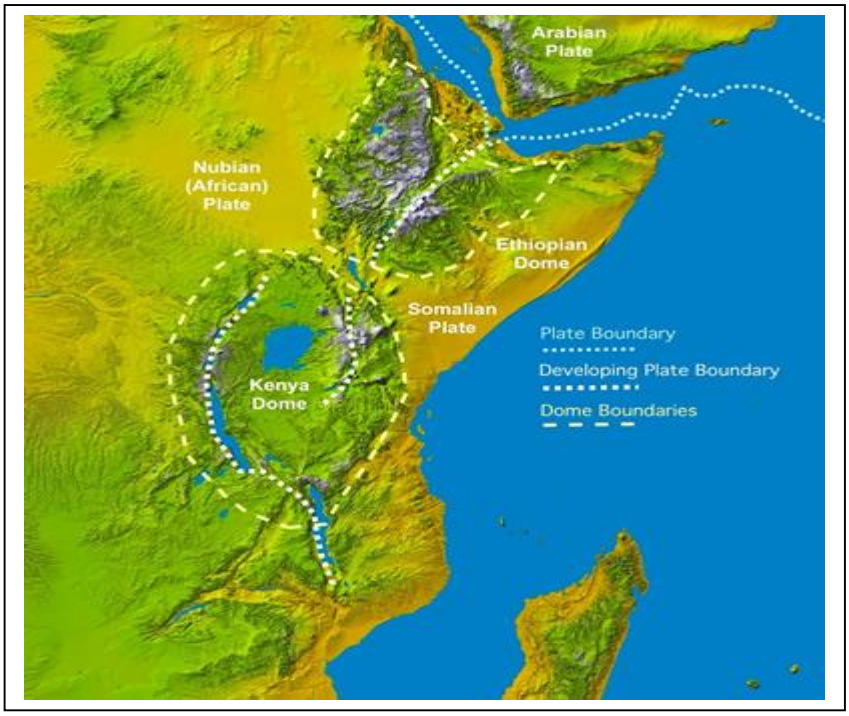

Figure1.1. Colored Digital Elevation Model showing tectonic plate boundaries outlines of the elevation highs demonstrating the thermal bulges and large lakes of East Africa.

The Main Ethiopian Rift (MER) is a symmetrical graben with uplifted flanks and steep border faults (Gidey et al, 1990). This structural depression serves as a divide between the northwestern or Ethiopian Plateau and southeastern or Somalian Plateau. This rift is believed to be the result of tensional movements that affected the uplifted Ethio-Somalia plateau (Di Paola, 1992; Mohr, 1986). A large number of step faults have produced a total difference in altitude of more than 1000m between the top of the plateau and the floor of the rift. Almost all the faults are normal faults (Di Paola, 1972).

The floor of the MER is marked by a persistent belt of intense, fresh, faulting which has been termed the Wonji Fault Belt (WFB) (Mohr, 1960). The WFB extends from south of Lake Chamo in southern Ethiopia to the Lake Abhe area in central Afar.

Two main tectonic events have been recognized concerning the tectonic evolution of the Ethiopian Rift System. The first event that started since Eocene (Mohr, 1976a) involved the uplift of the Ethiopian swell. Large scale faulting later took place across the swell to form the Afar and the Ethiopian Rift and this represents the second major tectonic events. The initiation of the Ethiopian Rift and the Afar can be traced to 14 Ma (Kazmin and Habtemichael, 1978). The last major episode of rift faulting resulted in the formation of the Wonji Fault Belt which is constituted by a number of faults which shattered the rift floor in to several relatively small horst and graben structures.

The Ethiopia Rift System, which represents the northern half of the East African Rift system (EARS), consists of three major rift zones with distinct volcanic and tectonic characteristics that are at different stages of rifting. These are the broadly rifted zone of southwestern Ethiopia, the Main Ethiopian Rift (MER) of central Ethiopia, and the Afar Rift Systems. The width of MER increases from the southern (30-60km) to the central (65-90km) and the northern (80-120km) sectors, and is more than 200km wide in the southern part pf the Afar Rift. The MER may be geographically subdivided into three sectors Northern, Central and Southern (Gidey et al, 1990). According to this subdivision the study area is located in the tectonically active central part of the Main Ethiopian Rift.

The four main lakes: Ziway, Abayata, Langano, and shala are believed to have been formed by volcano-tectonic processes. The first three lakes have an elongated shape parallel to the main trend of the MER and can be defined as tectonically controlled lakes. Unlike the other three lakes; Shala occupies caldera. The western part of the lake lies in a tectonically controlled depression. Thus, Lake Shala can be classified as volcanically-tectonically controlled lake. As a result of differences in the geomorphologic setting they vary considerably in depth, shape, and size.

Lake Langano is located 200km south of Addis Ababa and it is 7°36′ N and 38°43′ E, which occupies a large depression bounded by a well defined major fault system. The eastern and western shores are bounded by a graben, where as the northern part ends up as a small circular caldera in Oitu Bay and the southwestern and northern shores lap against the horst and grabens of the Wonji Fault Belt. The lake is fed by direct precipitation of the lake surface, hot springs and a number of small streams running from the highlands to the east and south of it. Contrary to that it discharges to Lake Abiyata through Horakelo river. It has average annual surface water and precipitation inflow of 461mcm and a combined annual average water loss from river run off and evaporation of 509mcm. But regardless of the above differences, water balance of the lake level remains stable indicating the contribution of groundwater flow to the lake through springs and escape through large faults (Tenalem Ayenew, 1998)

Lake Shala is located about the same distance as Lake Langano south of the capital city and its coordinate is 7°29′ N and 38°32′ E, which is one of the deepest lake in the Eastern African Rift System, occupying a major volcano-tectonic collapse modified by later regional faulting (Mohr, 1966; as cited in Di Bois. 1976). The major inflow comes from precipitation, surface run off through rivers Dijo and Awade, and hot springs around the shore. It has an average annual surface inflow of 535mcm and the only loss of water from the lake is through evaporation accounting to an average yearly total of 781mcm. The stable lake level

irrespective of the difference of the input and loss from the lake dictates the contribution of large amount of ground water inflow (Tenalem Ayenew, 1998)

This work is not the detailed study, but it will give some initial information for the future detailed studies in the area. The aim of the work is to investigate the possible ground water flow from the lake Langano to lake Shala as there exists elevation difference as well as mapping major structures (such as faults, dykes etc.) and defining the vertical stratification of the study area by using geophysical methods.

Table 1.1: Basic morphometeric data of the two lakes (Tenalem Ayenew, 2003)

Lake	Altitude (m.s.l)	Lake area(km^2)	Catchment area(km^2)	Maximum depth(m)	Mean depth(m)	Volume ($10^6 m^3$)
Langano	1585	230	2000	47.9	17	3800
Shala	1550	370	2300	266	8.6	3700

1.2 LOCATION OF THE STUDY AREA

The study area is located in the central part of the Main Ethiopian Rift within the limits of $38^0 32`$ - $38^0 43`$ east longitude and $7^0 29`$ - $7^0 36`$ north latitude (Figure 1.2). It is located about 200km south of the capital Addis Ababa and is about 40km south west of the Ziway town. Approximately it covers about 56.57 square kilometers. This area comprises several villages namely:Hada, Kore, Boso, Kerara which are found south west of lake Langano in which line 1 is located and others like Gale, Adele and Ajewa are found north east of lake Shala where line 3 is located. In addition to these Dole is located along the asphalt roadside. The study area is accessible with asphalt road as well as on dry weather road and on foot.

1.3 RELEVANCE OF THE STUDY

The Ethiopian Rift System (ERS) is one of the most interesting geologically studying areas in the world. Lakes Langano and Shala are the well known of the many lakes which are found in the Main Ethiopian Rift (MER) for their recreation purposes. Studying their possible connections for the flow of groundwater and structurally mapping the geology of the area between them will provide very important initial information on understanding of the groundwater potential of the area. Concerning hydrology, the result of this study will give good picture for further studies to know the possible movement of groundwater between the two lakes. The study also contributes towards the choice for the appropriate locations for construction of

infrastructures for the future such as for buildings and roads in the area. In addition to this, the study is vital for future detailed researches over the area.

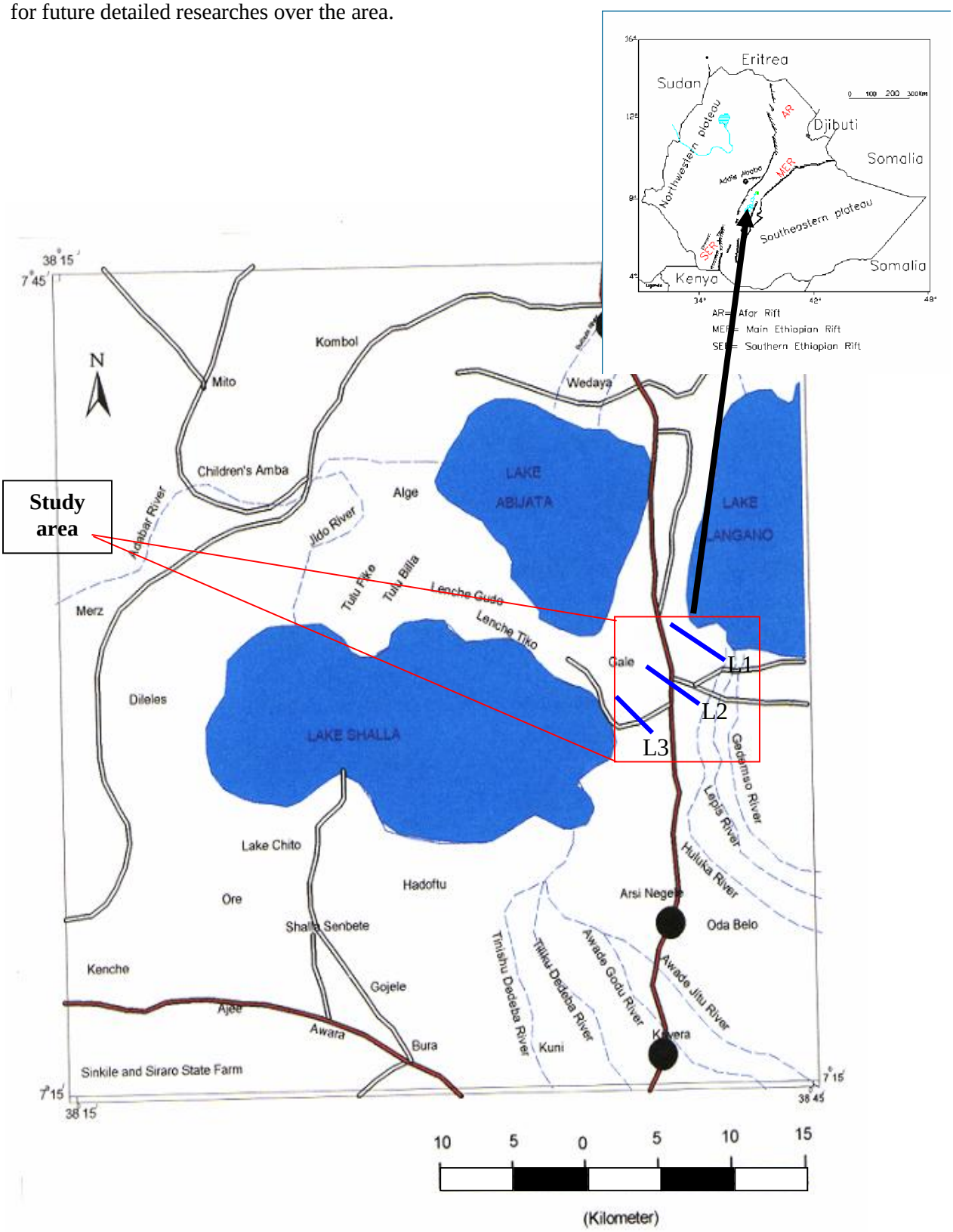

Figure 1.2. Location map of the study area

1.4 OBJECTIVES OF THE STUDY

General objective

- Geophysical investigations over the corridor between the Lakes Langano and Shala to understand the general subsurface condition of the area.

Specific objectives

- Defining the vertical geoelectric stratification of the area between the two lakes with a view to determine the existence of water bearing horizons and their depth.
- Mapping subsurface structures between the two lakes that may connect the two lakes and could possibly be conduits for flow of underground water.
- Familiarizing oneself with practical methodologies of geophysical data acquisition, data analysis and interpretation

1.5 GENERAL OVERVIEW OF THE STUDY

On this thesis there are five chapters. The first chapter contains the general introduction about the study. The thesis also explains about the three basic geophysical methods employed for this particular work in chapter two. Chapter three discusses mainly about data acquisition, processing and presentation. Following this, results and interpretations are presented in chapter four. Finally discussion, conclusions and recommendations are forwarded in chapter five.

1.6 GEOLOGY OF THE STUDY AREA

Geology of the Main Ethiopia Rift

The tectonic and volcanic activities that took place during the Cenozoic were significant in the making of the rift. The general succession of the strata in the horn of Africa consists of a Precambrian sequence mainly of metamorphic, Mesozoic sedimentary sequence, Tertiary flood basalts and silicic lava flows with pyroclastic sediments interstratified overlain by Quaternary sediments and alkali silicic lava flows (Mohr, 1971). At the beginning of the Mesozoic era a shallow sea spread occurred over much of Ethiopia as a result of land subsidence. As the land continued to subside different types of deposits were accumulated in different places over the Precambrian basement rocks. Following the Mesozoic era there was extensive magmatism and faulting which modified the face of the East Africa.

The Ethiopian rift system was formed by extensional tectonics (Mohr, 1967; Kazmin and Habitemichael Berhe, 1978). Rifting in this part of the world started during the early Tertiary period jointly with regional crustal uplift forming the Afro-Arabian dome until the end of the Eocene.

The opening of the Ethiopian Rift is related to the uprising of at least two mantle plumes, presently located beneath the central Gregory Rift in Kenya and beneath the Afar depression. The older Kenyan plume gave rise to the Eocene–Oligocene magmatism of Southern Ethiopia (Yemane et al, 1999), which successively migrated southward as a consequence of northward movements of the African plate. The Afar plume is believed to be younger and responsible for the bulk of the magmatism in the central Ethiopia and Afar region (Morley, 1999). From Oligocene to the earliest Miocene following the uplift of the Afro-Arabian dome, basaltic magma eruptions occurred through fissures in tensional zones (Mohr, 1962a, and 1971b). The rift faulting following the capacious trap volcanics split the crust in to three distinct segments: the Arabian plate, the African plate and the Somalian plate (Mohr, 1971b). The central part of this rift system is called the Main Ethiopian Rift (MER).

A rather simplified geologic map of the major part of the MER is given in Figure 1.3 (Tenalem Ayenew, 1998). The major rock units as indicated in the figure are recent basaltic flows, ignimbrites, rhyloites and lake sediments. Some of these geologic units are also intercepted by some main boreholes drilled over the study area (Tables 1.1).

By late Miocene, the eastern and western faulted margins of the rift had formed. In early Pliocene, evolution from alternating half grabens to a full, symmetrical graben occurred (Wolde Gabriel, 1987). The subsequent volcanic activity of the rift has been largely confined to the active Wonji Fault Belt (WFB) running parallel to the rift axes (Mohr, 1967; Baker et al, 1972). The Wonji Fault Belt has 5-12 Km width and maintains a NNE orientation along the entire length of the MER. The WFB has been forced into en-echelon offsets in order to remain within the rift margin envelope (Mohr, 1980).

There is a general agreement among researchers about the existence of a single, huge ancestral lake covering much of the MER. The major rift lakes are the shrunken remnants of this large lake dating back to the Miocene (Tenalem, 1998). Sediments of lacustrine origin cover some areas of the rift with varying thickness and some fluvial and colluvial deposits also found about the lakes region.

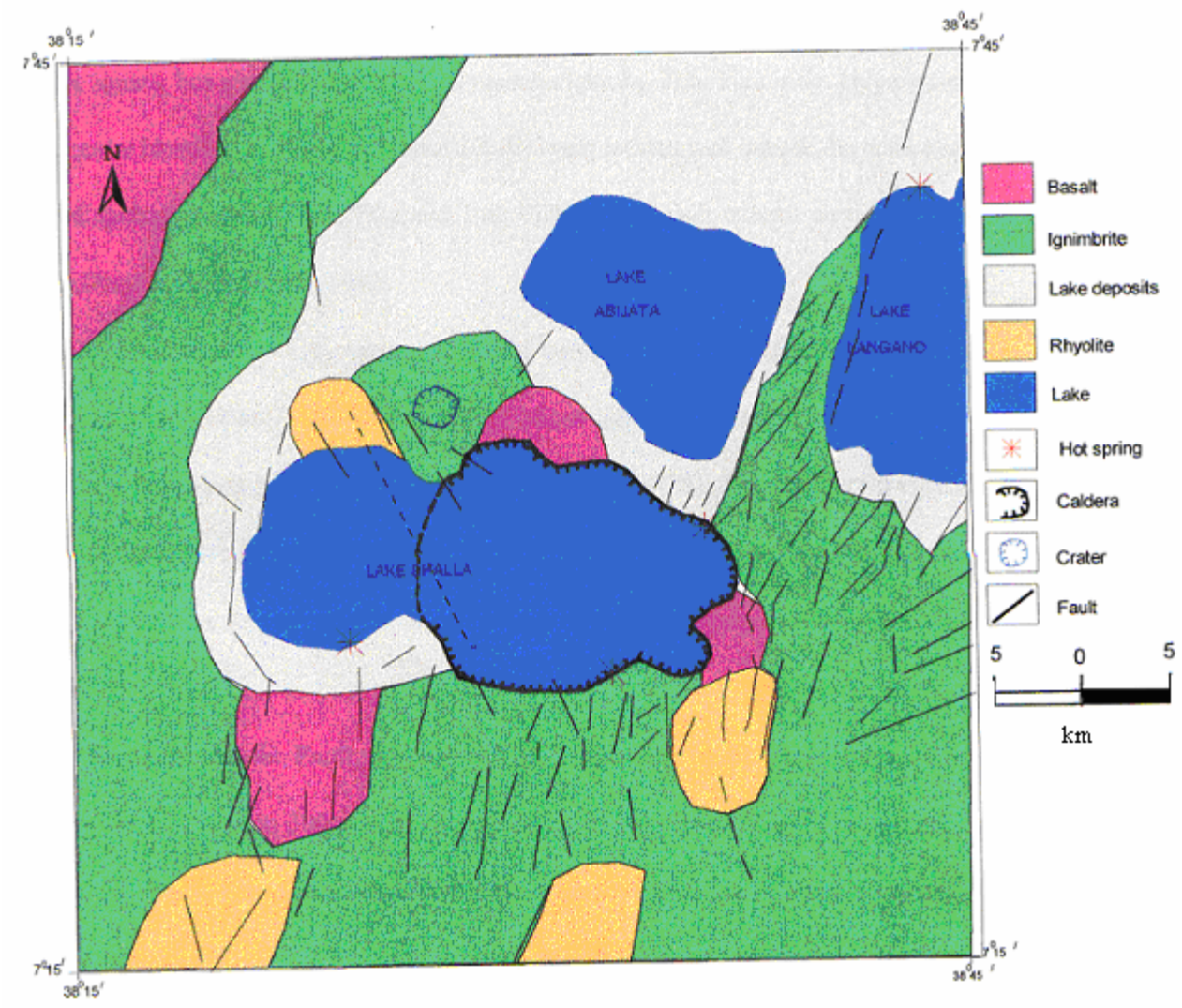

Figure 1.3 Geological map of the study area.

Table 1.2: Bore hole information around the study area.(Tesfaye Cherinet, 1982)

Borehole locations	Elevation (m)	Total Depth (m)	Lithology
Negelle Arsi (Sinor Gino)	1920	93	Volcanic sand
Negelle Arsi (Municipality)	1920	109	Volcanic sand
Langano (Bekele Mola)	1597	15	Shore sand
Dole (Wildlife Conservation)	1630	116.6	Ignimbrite
NW of Langano	1583	-	Lacustrine sediment
Between Lake Abiyata and Langano	1626	56.5	Lacustrine sediment
Bulbula	1605	71	Lacustrine sediment

CHAPTER TWO

GEOPHYSICAL METHODS

2.1 THE DIRECT CURRENT RESISTIVITY METHOD

The electrical resistivity method is based on the principle of applying artificially generated electric current to the Earth through two electrodes (called source and sink) and measuring the potential difference between two other electrodes (called potential electrodes). The distance between the electrodes and the measured potential difference are the data that can be used to make interpretations of the subsurface conditions of the particular study area.

Various materials differ in their ability to conduct electricity. In some materials at least one of the electrons in each atom is loosely held and it requires only slight external influence to move or conduct some of the electrons from atom to atom through the material. In other materials there are very few free electrons and they conduct electricity poorly. This type of electrical conduction is called electronic conduction. Metals are excellent electronic conductors while rocks are poor to very poor electronic conductors. Another form of electrical conduction is electrolytic conduction, where the current is carried by ions, such as in mineralized ground water, resulting in actual movement of matter.

In electrical resistivity investigations both types of electrical conductivity are involved; electronic conductivity through the soil particles and rock where as electrolytic conduction in the ground water.

2.1.1 Fundamental Principle of DC Resistivity

The purpose of electrical survey is to determine the subsurface resistivity distribution by making measurements on the ground surface. From these measurements, the true resistivity of the subsurface can be estimated.

The fundamental physical law that governs the flow of current in the ground; which states that "If a direct current is made to flow through a circuit element, then the ratio of the potential drop across the element to the current flowing through it is constant." The mathematical expression of this statement is given as

$$R = \frac{\Delta V}{I} \tag{2.1}$$

where ΔV is potential drop in volts

I is current in amperes and

R is resistance in ohms.

Resistivity

Considering a uniform electrical current flowing through a homogeneous cylindrical bar (figure 2.1) in the direction of its axis, the resistance will be proportional to the length (l) and inversely proportional to the cross sectional area (A) of the cylinder. Mathematically this can be written as

$$R = \frac{\rho\, l}{A} \tag{2.2}$$

The proportionality constant ρ (Ohm meter) is called Resistivity. It is the relative ability of materials to resist electricity when a voltage is applied. The resistivity of a material is fundamental property of that material and is independent of the dimension.

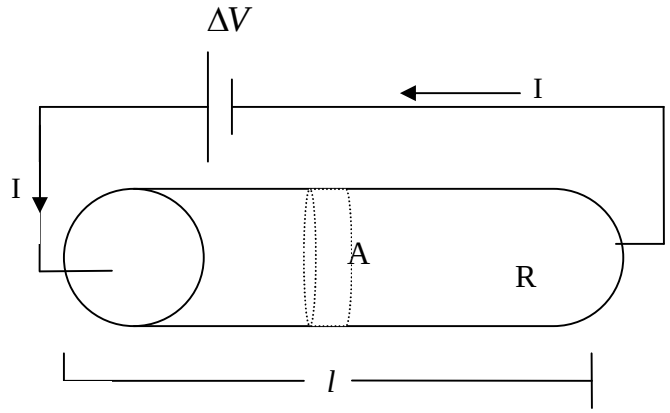

Figure 2.1 Parameters used in defining resistivity

In more generalized form we can consider the current density field $\vec{J}$ instead of the total current I flowing through a finite volume; and electric potential gradient $\vec{E}$ instead of the potential drop. Hence equation (2.1) can be written as:

$$R = \frac{\Delta V}{I} = \frac{l\vec{E}}{A\vec{J}} = \left(\frac{\vec{E}}{\vec{J}}\right)\frac{l}{A} \tag{2.3}$$

Comparing equation (2.2) and (2.3) we came up with the following expression.

$$\vec{J} = \frac{\vec{E}}{\rho} \tag{2.4}$$

This equation is the vector form of Ohm's Law for current flow in a continuous medium. The inverse of resistivity ($\sigma = 1/\rho$) is called electrical conductivity with the unit of siemens pre meter (S/m).

Equation (2.4) can also be written in terms of conductivity as

$$\vec{J} = \sigma\vec{E} \tag{2.5}$$

An electrically isotropic medium is the one for which the resistivity ρ, is a scalar function of the point of observation and the current density $\vec{J}$, is in the same direction as the electric field vector $\vec{E}$. Hence both equation (2.4) and (2.5) are applied to isotropic medium.

In an anisotropic medium, $\vec{J}$ has a directive property and, in general, is not in the direction of $\vec{E}$. Mathematical we can express this as

$$\vec{J}_i = \sigma_{ik}\vec{E}_k \tag{2.6}$$

Where the conductivity (σ_{ik}) now appears not as a scalar, but as second rank tensor. Equation (2.6) can also be written as

$$\left.\begin{aligned} J_x &= \sigma_{xx}E_x + \sigma_{xy}E_y + \sigma_{xz}E_z \\ J_y &= \sigma_{yx}E_x + \sigma_{yy}E_y + \sigma_{yz}E_z \\ J_z &= \sigma_{zx}E_x + \sigma_{zy}E_y + \sigma_{zz}E_z \end{aligned}\right\} \tag{2.7}$$

When $\sigma_{xx} = \sigma_{yy} = \sigma_{zz} = \sigma$ and all other components of σ_{ik} vanished it reduces to the isotropic case.

The electric field is conservative and hence the electric field intensity $\vec{E}$ is related to the gradient of the a scalar potential,

$$\vec{E} = -\nabla \cdot V \tag{2.8}$$

Thus using equation (2.4) we have

$$\vec{J} = -\frac{1}{\rho}\nabla \cdot V \tag{2.9}$$

If the charge is conserved within a volume enclosed by a surface S, we will have the following integral form

$$\oint_s J.ds = 0 \tag{2.10}$$

Gauss theorem states that the volume integral of the divergence of the current throughout a given region is equal to the total charge enclosed, so that in this case, we have

$$\int_v (\nabla \cdot J)\, dv = 0 \tag{2.11}$$

Taking v as an infinitesimal volume element enclosing a given point, we get for this point the following expression

$$\nabla \cdot J = -\nabla \cdot \nabla(\frac{V}{\rho}) = 0 \ ,$$

Hence
$$\nabla\left(\frac{1}{\rho}\right) \cdot \nabla V + \frac{1}{\rho}\nabla^2 V = 0 \tag{2.12}$$

For homogeneous medium ρ is independent of coordinates so that equation (2.12) reduces to

$$\nabla^2 V = 0 \tag{2.13}$$

This equation is the Laplace equation and has different forms in different coordinate systems:

- In Cartesian coordinates

$$\frac{\partial^2 V}{\partial x^2} + \frac{\partial^2 V}{\partial y^2} + \frac{\partial^2 V}{\partial z^2} = 0 \tag{2.14}$$

- In cylindrical coordinates

$$\frac{\partial^2 V}{\partial r^2} + \frac{1}{r}\frac{\partial V}{\partial r} + \frac{\partial^2 V}{\partial z^2} + \frac{1}{r^2}\frac{\partial^2 V}{\partial \theta^2} = 0 \tag{2.15}$$

- In spherical coordinates

$$\frac{1}{r^2}\frac{\partial}{r}\left(r^2 \frac{\partial V}{\partial r}\right) + \frac{1}{r^2 \sin\theta}\frac{\partial}{\partial \theta}\left(\sin\theta \frac{\partial V}{\partial \theta}\right) + \frac{1}{r^2 \sin^2\theta}\frac{\partial^2 V}{\partial \phi^2} = 0 \tag{2.16}$$

2.1.2 General Equation for Electrical Potential

Potential due to a single current electrode at depth

Now let us consider a homogeneous and isotropic medium in which the current source is buried at depth. The current circuit is completed through another electrode at larger distance so as to neglect its influence (Figure 2.2).

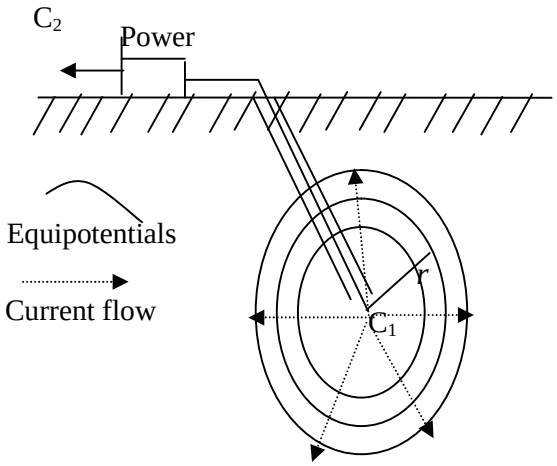

Figure 2.2 Buried point source of current in homogeneous ground

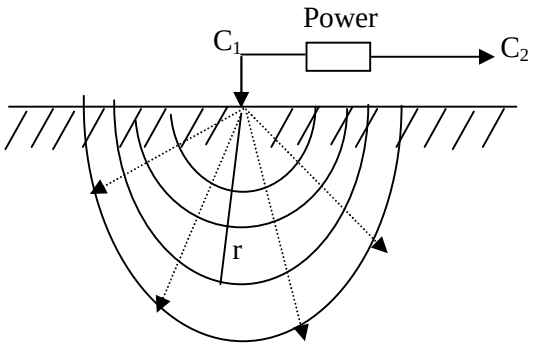

Figure 2.3. Point source at the surface of the ground

For spherical current distribution (figure 2.3), the potential will be a function of r only, where r is the distance from the source C_1 to any equipotential surface. Under these conditions the Laplace equation (2.13), in spherical coordinates will be our concern. Here $\frac{\partial V}{\partial \theta}$ and $\frac{\partial V}{\partial \phi}$ are zero since the potential is only the function of r. Therefore equation (2.16) reduces to

$$\frac{1}{r^2}\frac{d}{dr}\left(r^2\frac{dV}{dr}\right)=0 \Rightarrow r^2\frac{dV}{dr}=A \Rightarrow \frac{dV}{dr}\frac{A}{r^2} \tag{2.17}$$

wehere A is arbitrary constant. Integrating (2.17), we get

$$V=-\frac{A}{r}+B \tag{2.18}$$

Where B is also another arbitrary constant. Because V=0 when $r \to \infty$, we get B=0. The total current crossing a spherical surface of radius r is given by

$$I=4\pi r^2 J \tag{2.19}$$

and equation (2.9) for this case (radial) becomes,

$$J = \frac{-1}{\rho}\frac{dV}{dr} \tag{2.20}$$

This implies that, from (2.18) and (2.19) we can have the following expression for the constant A:

$$A = \frac{-I\rho}{4\pi} \tag{2.21}$$

Finally using (2.18) and (2.21), the potential at a distance r is given by

$$V = \frac{I\rho}{4\pi r} \tag{2.22}$$

Potential due to a single current electrode on the surface of the Earth

For homogeneous hemispherical ground section of resistivity ρ (figure 2.3), the current distribution at a distance r becomes $I = 2\pi r^2 J$. Following the same steps as above the potential at radial distance becomes

$$V = \frac{I\rho}{2\pi r} \tag{2.23}$$

Four-electrode resistivity layout

In electrical resistivity surveys the current I is injected in to the subsurface through a pair of electrodes (source and sink), and the resulting potential difference ΔV , is measured by means of another pair of electrodes know as potential probes (electrodes).

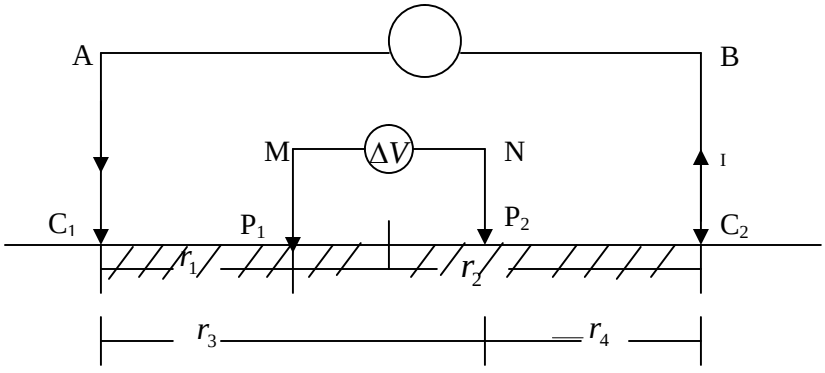

Figure 2.4 Four-electrode configurations.

When the distance between the two current electrodes is finite (figure 2.4) above, the potential at any nearby surface point will be affected by both current sources (C_1 and C_2 electrodes). Using the result of equation (2.23), the potential at P_1 due to C_1 and C_2 can be given as

$$V_1 = \frac{I\rho}{2\pi}\left(\frac{1}{r_1} - \frac{1}{r_2}\right) \tag{2.24}$$

Likewise, the potential at P_2 due to C_1 and C_2 becomes

$$V_2 = \frac{I\rho}{2\pi}\left(\frac{1}{r_3} - \frac{1}{r_4}\right) \tag{2.25}$$

Hence, the potential difference between P_1 and P_2, ΔV due to the current I, is given by

$$\Delta V = V_1 - V_2 = \frac{I\rho}{2\pi}\left[\left(\frac{1}{r} - \frac{1}{r_2}\right) - \left(\frac{1}{r_3} - \frac{1}{r_4}\right)\right] \tag{2.26}$$

Equation (2.26) can be written as

$$\rho = \frac{K\Delta V}{I} \tag{2.27}$$

where $K = 2\pi\left[\frac{1}{\frac{1}{r_1} - \frac{1}{r_2} - \frac{1}{r_3} + \frac{1}{r_4}}\right]$; is the **geometric factor** and depends only on the electrode arrangement.

2.1.3 Common Electrode Configurations

There are various electrode arrangements used in electrical measurements so that the apparent resistivity can be determined. Among the most widely used, two of the configurations commonly applicable in DC resistivity surveys are the following:

1. The Wenner Array

This array is a symmetrical arrangement in which the points A, M, N and B are taken on a straight line such that the points are symmetrically placed at a fixed separation 'a'.

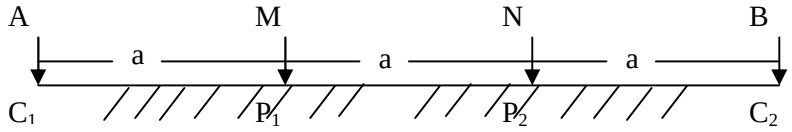

Figure 2.5 Electrode arrangements for Wenner array

Here $r_1 = a$, $r_2 = 2a$, $r_3 = 2a$ and $r_4 = a$. Substituting the above values in equation (2.27), we get $\Delta V = \frac{I\rho}{2\pi}\left(\frac{1}{a}\right)$ So that

$$\rho_a = 2\pi a\left(\frac{\Delta V}{I}\right) \tag{2.28}$$

where K= $2\pi a$ is the geometric factor of the Wenner array.

2. The Schlumberger Array

The Schlumberger array is also a symmetrical arrangement in which A, M, N and B are taken on a straight line such that the points are symmetrically placed about the center of the spread O (figure 2.6). When this arrangement is used for sounding, the MN separation in kept constant for a number of AB values, which are successively increased for larger depth penetrations. Nevertheless, when the value of MN, in comparison to AB, becomes too small and the potential drops significantly to be measured precisely, it needs to be increased accordingly.

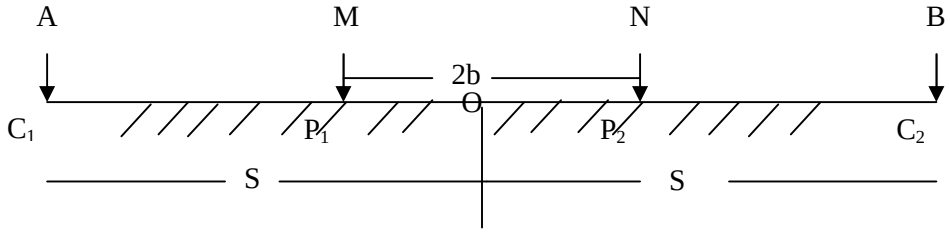

Figure 2.6 The Schlumberger array arrangement.

Here r_1 = S-b, r_2 = S+ b, r_3 = S+ b and r_4 = S-b. Substituting these values in to equation (2.27) and simplification gives

$$\Delta V = \frac{I\rho}{2\pi}\left[\frac{2b}{S^2 - b^2}\right], S >> b$$

So that the apparent resistivity becomes

$$\rho_a = \pi \frac{\left(S^2 - b^2\right)}{2b}\left(\frac{\Delta V}{I}\right) \tag{2.29}$$

where $K = \pi \frac{\left(S^2 - b^2\right)}{2b}$, is the geometric factor for this array.

2.1.4 Electrical Survey Practice

There are two types of field operations in electrical surveys depending on the desired information.

Resistivity Sounding

In resistivity sounding, which is also know as Vertical Electrical Sounding (VES), the positions of electrodes changed with respect to a fixed point (known as the sounding point) and the measured values reflect the vertical distribution of resistivity values on a geologic section.

Resistivity Profiling

In resistivity profiling, the value of K remains constant for a particular set of readings measurements are done along a straight line, at successive points, on the surface. In this way, we get the lateral variations of resistivity at a certain depth level.

2.1.5 Principle of Equivalence and Suppression

The principle of equivalence and suppression introduce ambiguity and a non-unique solution in electrical resistivity interpretations. Equivalence refers to the condition in which different combination of layer resistivity and thickness may lead to apparent resistivity curves, which are within the accuracy of observation. As well as these curves are indistinguishable although not identical.

Whereas suppression refers to the condition in which the effect of an intermediate layer (thickness very small compared to its depth) in apparent resistivity curve of ascending and descending type is small that its detection from the curve may be impossible.

There are different types of equivalence:

1. For $h_2 < h_1$, $\rho_2 < \rho_1$ and $\rho_3 > \rho_2$, theoretical computation of the potential for a three layer section shows that, the result does not depend on the individual values of the parameters of the intermediate layer but only on the ratio h_2/ρ_2=S. This is referred to as H-type equivalence i.e., if the resistivity and thickness of the intermediate layer are changed within a certain range, keeping the conductance (=conductivity x thickness) constant, the observed apparent resistivity curve remains invariant, within the acceptable margin of observational error. Since both H- and A- type sections satisfies the condition that $\rho_3 > \rho_2$, they may be called equivalent with respect to S.
2. For $h_2 < h_1$; $\rho_2 >> \rho_1$ and $\rho_3 < \rho_2$, the value of the potential depends only the product $h_2 \rho_2 = T$. This is referred to as K-type of equivalence in which the shape of the curve remains invariant as far as the transverse resistance, *T*, is kept more or less constant. And, as both K- and Q- type sections satisfies the condition that $\rho_3 < \rho_2$, they may be called equivalent with respect to T.

2.1.6 Electrical Properties of Earth Materials

The resistivity of common rocks and soil materials (Telford et al. 1990) is shown in Figure 2.7.Igneous and metamorphic rocks typically have high resistivity values. The resistivity of these rocks is greatly dependent on the degree of fracturing, and the percentage of the fractures filled with ground water. Thus a given rock type can have a large range of resistivity, from about 1000 to 10 million Ωm, depending on whether it is wet or dry. This characteristic is useful in the detection of fracture zones and other weathering features, such as in engineering and groundwater surveys.

Sedimentary rocks, which are usually more porous and have higher water content, normally have lower resistivity values compared to igneous and metamorphic rocks. The resistivity values range from 10 to about 10000 Ωm, with most values below 1000 Ωm. The resistivity values are largely dependent on the porosity of the rocks, and the salinity of the contained water.

Unconsolidated sediments generally have even lower resistivity values than sedimentary rocks, with values ranging from about 10 to less than 1000 Ωm. The resistivity value is dependent on the porosity (assuming all the pores are saturated) as well as the clay content. Clayey soil normally has a lower resistivity value than sandy soil. However, note the overlap in the resistivity values of the different classes of rocks and soils. This is because the resistivity of a particular rock or soil sample depends on a number of factors such as the porosity, the degree of water saturation and the concentration of dissolved salts.

The resistivity of groundwater varies from 10 to 100 Ω m. depending on the concentration of dissolved salts. Note the low resistivity (about 0.2 Ω m) of seawater due to the relatively high salt content. This makes the resistivity method an ideal technique for mapping the saline and fresh water interface in coastal areas. One simple equation that gives the relationship between the resistivity of a porous rock and the fluid saturation factor is Archie's Law. It is applicable for certain types of rocks and sediments, particularly those that have low clay content. The electrical conduction is assumed to be through the fluids filling the pores of the rock. Archie's Law is given by

$$\rho = a\rho_w \phi^{-m} \tag{2.30}$$

where ρ is the rock resistivity, ρ_w is fluid resistivity, ϕ is the fraction of the rock filled with the fluid, while "a" and "m" are two empirical parameters. For most rocks, "a" is about 1 while m is about 2.

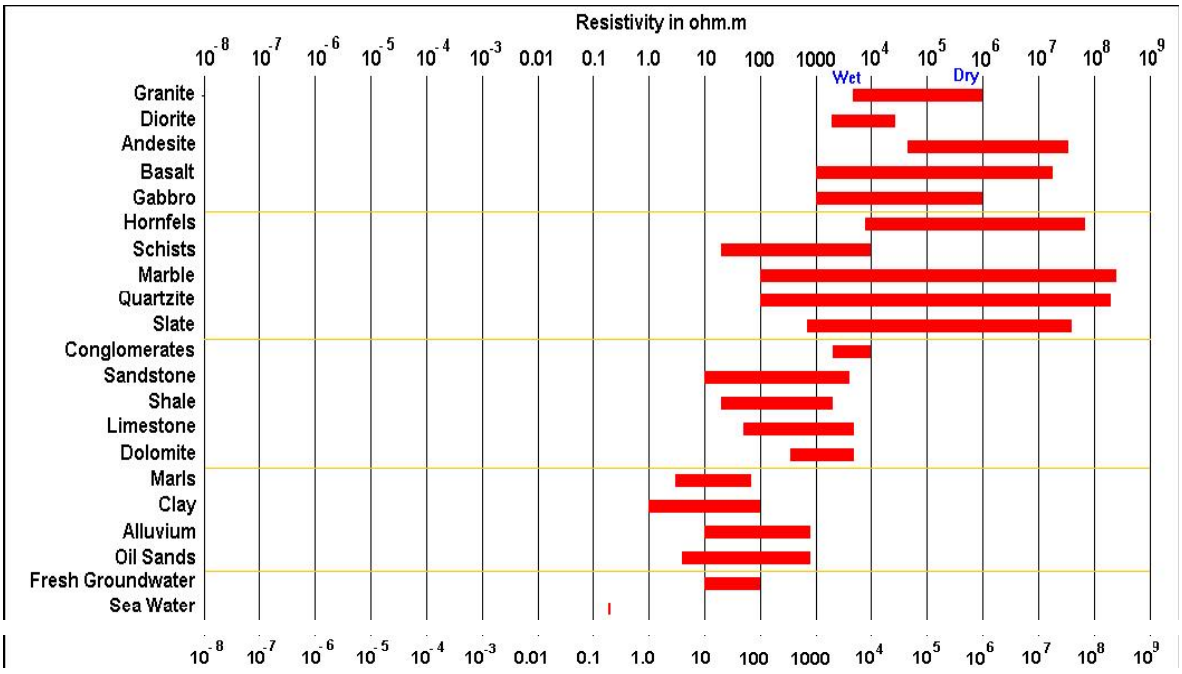

Figure 2.7 The resistivity of rocks and soils.

2.2 THE GRAVITY METHOD

In exploration geophysics, the gravity method exploits the earth's field difference caused by lateral density variations in the earth's crust. If geologic movements causes in the dislocation of rocks of different densities, the resulting indiscretion in lateral density distribution will make corresponding variation in the intensity of gravity. The measured variation in the earth's gravity field is interpreted as convincing subsurface mass distributions. The gravity method is also used in modeling the earth's crust, in locating area of anomalous mantle materials (in areas of plate margins) and it is the basis for the study of the earth's shape (Telford, 1990)

2.2.1 Fundamental Principle

Gravity Survey is measurements of the gravitational field at a series of different locations over an area of interest. The objective in exploration work is to associate gravity variations with differences in the distribution of densities and hence rock types.

Geophysical interpretations from gravity surveys are based on the mutual attraction experienced between two masses as first expressed by Isaac Newton. Newton's law of gravitation states that "the mutual attractive force between two point masses, m_1 and m_2, is inversely proportional to the square of the distance between them". The constant of proportionality is usually specified as *G*, **the universal gravitational constant**.

Thus, we usually see the law of gravitation written as shown bellow where $\boldsymbol{F}$ is the force of attraction, $G = 6.67x10^{-11}\ Nm^2/Kg^2$ is the gravitational constant, and *r* is the distance between the two masses, m_1 and m_2.

$$\boldsymbol{F} = \frac{Gm_1m_2}{r^2} \tag{2.31}$$

When making measurements of the earth's gravity, we usually don't measure the gravitational force, *F*. Rather; we measure the gravitational acceleration, *g*. The gravitational acceleration is the time rate of change of a body's speed under the influence of the gravitational force.

$$F = m_2 g \tag{2.32}$$

In addition to defining the law of mutual attraction between masses, Newton also defined the relationship between a force and acceleration. Newton's second law states that force is proportional to acceleration. The constant of proportionality is the mass of the object.

$$g = \frac{Gm_1}{r^2} \tag{2.33}$$

Combining Newton's second law with his law of mutual attraction, the gravitational acceleration on the mass m_2 can be shown to be equal to the mass of attracting object, m_1, over the squared distance between the two masses, r.

2.2.2 Gravitational Potential of the Ellipsoidal Earth

By virtue of its position in the gravitational field of the earth, a mass m has gravitational potential energy U. The gravitational potential energy U of the mass m at distance r from the earth's mass M that is assumed to be concentrated at its center is given by:

$$U = \frac{GMm}{r} \tag{2.34}$$

If the test mass m moves to a new position r' from M, the gravitational energy that is released as

$$\Delta U = \frac{GMm}{r'} - \frac{GMm}{r} \tag{2.35}$$

This released energy can be regarded as the negative of the work done on m by the gravitational force of attraction in bringing m from infinity to its position in the earth's gravitational field.

The gravitational potential V is defined as the potential energy of m divided by its mass that is:

$$V = \frac{U}{m} = \frac{GM}{r} \tag{2.36}$$

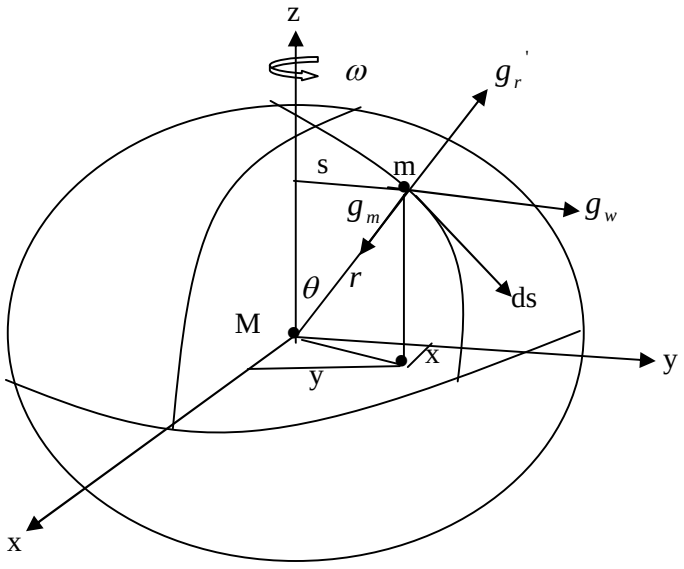

Figure 2.8 Relationship between Cartesian and spherical coordinates for the derivation of the Gravitational Potential of the Ellipsoidal Earth.

Because the gravitational field is conservative, the potential energy per unit mass V depends only on the position in the gravitational field and not on the path through which a mass is brought to the location.

The earth's gravity potential or the geopotential W at the earth's surface consists of the mass gravitational potential V generated by all masses of the earth and the rotational (Centrifugal) potential φ resulting from the radial component g'_r of the centrifugal acceleration g_w acting in these masses because of there rotation. Hence the geopotential is given by:

$$W = V + \varphi \tag{2.37}$$

From the above figure (2.8) the centrifugal potential φ can be determined as

$$\varphi = \frac{1}{2}\omega^2 s^2 = \frac{1}{2}\omega^2\left(x^2 + y^2\right) \tag{2.38}$$

Since $s = r\sin\theta$, (2.38) can be expressed in terms of spherical coordinates as

$$\varphi = \frac{1}{2}\omega^2 s^2 = \frac{1}{2}\omega^2 r^2 \sin^2\theta \tag{2.39}$$

The explicit form of the earth's gravity potential or geopotential W on the earth's surface is expressed as:

$$W = V + \varphi = \int G\frac{dm}{r} + \frac{1}{2}\omega^2\left(x^2 + y^2\right) \tag{2.40}$$

The change in the earth's potential, dW when the test mass m is displaced by an amount dr along r is equal to the work done by the earth's gravitational field given by

$$dW = \vec{g}.d\vec{r} \Rightarrow W = -\int \vec{g}\cdot d\vec{r} \tag{2.41}$$

If the test mass is moved in a direction perpendicular to g then the integral in (2.41) results in a constant value. Therefore,

$$W = C \tag{2.42}$$

Equation (2.42) defines a family of equipotential surface, each of which can be determined by assigning a definite (particular) value to the constant C. Of theses family of equipotential surfaces, the ellipsoid and the geoid are two of such equipotential surface of the earth that are constructed to coincide with a theoretical earth model (ellipsoid) and the physical earth model (geoid). Geophysicists and geodesists consider these two surfaces to represent the average shape of the rotationally distorted real earth.

2.2.3 Theoretical Gravity of the Earth

The shape of the earth, based on geodetic measurements and recent satellite tracking, is practically thought to be spheriodal, bulging at the equator and flattened at the poles with the ellipticity given by

$$\frac{R_e - R_p}{R_e} = \frac{1}{298.25} \tag{2.43}$$

Where $R_e = 6378.14Km$ is radius of the earth at the equator and $R_p = 6356.75Km$ is the radius of the earth at the pole, equation (2.43) also known as polar flattening.

The international reference ellipsoid is a mathematical surface and a close approximation to the equipotential surface of gravity. The theoretical value of gravity g_N on this rotating ellipsoid can be computed by differentiating the gravity potential W (2.40), that is

$$\vec{g}_N = \vec{\nabla} W \tag{2.44}$$

This yields the radial and transverse components of gravity, which are then combined by performing the required mathematics to determine the variation of the theoretical gravity value g_N that is normal to the ellipsoid surface which is given by

$$g_N = g_e\left(1 + \beta_1 \sin^2\phi + \beta_2 \sin^4\phi\right) \tag{2.45}$$

Where g_e the value of gravity at the equator, at zero latitude, $\beta_1 and \beta_2$ are constants determined by adjustment. Equation (2.45) is known as the normal gravity formula. The normal gravity formula also known as theoretical gravity formula is very important in the analysis of gravity measurements on the Earth, because it gives the theoretical variation of normal gravity with latitude on the surface of the reference ellipsoid.

In 1967, the IUGG (International Union of Geophysics and Geodesy) adopted a revised theoretical gravity formula given by

$$g_N = 978031.85\left(1 + \beta_1 \sin^2\phi + \beta_2 \sin^4\phi\right) mgal \qquad (2.46)$$

where ϕ = latitude

β_1 =0.005278895

β_2 =0.0023462

Equation (2.46) is called the 1967 geodetic reference system formula (GRS 67 formula). The GRS 67 formula is adequate for analysis of gravity survey results (Robinson, 1988). This formula tells us what we need to know about large-scale variations in gravity caused by flattening and rotation of the earth.

2.2.4 Gravity Corrections

Thus far we have shown how variations in the gravitational acceleration can be measured and how these changes might relate to subsurface variations in density. We've also shown that the spatial variations in gravitational acceleration expected from geologic structures can be quite small.

Because these variations are so small, we must now consider other factors that can give rise to variations in gravitational acceleration that are as large, if not larger, than the expected geologic signal. These complicating factors can be subdivided into two categories: those that give rise to temporal variations and those that give rise to spatial variations in the gravitational acceleration.

- ***Temporal Based Variations*** - These are changes in the observed acceleration that are time dependent. In other words, these factors cause variations in acceleration that would be observed even if we didn't move our gravimeter.

  ○ **Instrument Drift** - Changes in the observed acceleration caused by changes in the response of the gravimeter over time.

  ○ **Tidal Affects** - Changes in the observed acceleration caused by the gravitational attraction of the sun and moon.

- ***Spatial Based Variations*** - These are changes in the observed acceleration that are space dependent. That is, these change the gravitational acceleration from place to place, just like the geologic affects, but they are not related to geology.

  ○ **Latitude Variations** - Changes in the observed acceleration caused by the ellipsoidal shape and the rotation of the earth.

  ○ **Elevation Variations** - Changes in the observed acceleration caused by differences in the elevations of the observation points.

○ **Slab Effects** - Changes in the observed acceleration caused by the extra mass underlying observation points at higher elevations.

○ **Topographic Effects** - Changes in the observed acceleration related to topography near the observation point.

Instrument Drift Correction

Drift is a gradual and unintentional change in the reference value with respect to which measurements are made. Although constructed to high-precision standards and capable of measuring changes in gravitational acceleration to 0.01 mgal, problems do exist when trying to use a delicate instrument such as a gravimeter. These variations in spring properties with time can be due to stretching of the spring over time or to changes in spring properties related to temperature changes. To help minimize the later, gravimeters are either temperature controlled or constructed out of materials that are relatively insensitive to temperature changes.

This drift is corrected for by including base station readings in your survey. The base station is a reference station that is kept constant throughout a survey and is revisited ever 1 to 2 hours each day during a survey. These regular base station measurements are used to correct for drift variations. It is assumed that the drift components of the gravity field vary linearly between two base station readings, therefore the time-varying components of the gravity field can be easily predicted, and removed.

Tidal correction

Tidal Effect is the variations in gravity observations resulting from the attraction of the moon and sun and the distortion of the earth so produced. Superimposed on instrument drift is another temporally varying component of gravity. Unlike instrument drift, which results from the temporally varying characteristics of the gravimeter, this component represents real changes in the gravitational acceleration. Unfortunately, these are changes that do not relate to local geology and are hence a form of noise in our observations.

Modern gravimeters, such as sintrex CG-3, which is used for this study has a built in earth-tide correction that can remove tidal effects of the specific location by feeding the latitude and longitude of the area.

Latitude Correction

The two features of the earth's large-scale structure and dynamics affect out gravity observations are it shape and rotations. This combined effect of the earth produces an increase in the value of g with latitude. Generally g increases from $9.78 m/s^2$ at the equator to $9.83 m/s^2$ at the poles. The variation of gravity with latitude over the surface of an ellipsoidal earth can be expressed using the theoretical gravity formula GRS 1967 (2.46). The latitude correction dg_L is obtained by differentiating the theoretical gravity formula

$$\frac{dg_L}{ds} = \left(\frac{1}{R}\right)\frac{dg_\phi}{d\phi} = 0.811\sin(2\phi)mgal \text{ , N-S of the base station} \qquad (2.47)$$

where, R is the mean radius of the earth

ϕ = Geographical latitude

$ds = Rd\phi$ is N-S horizontal distance (in Km)

Since gravity increases with latitude (both N and S), the above correction is always additive as one goes towards the equator.

Free Area Correction

To account for variations in the observed gravitational acceleration that are related to elevation, we incorporate a correction to our date known as the Free-Air Correction. In applying this correction, we mathematically convert our observed gravity values to ones that look like they were all recorded at the same elevation, thus further isolating the geological component of the gravitational field.

Note that the gravitational attraction decreases with elevation since it varies inversely with the square of the distance from the earth's center. Hence, it is necessary to correct the reading so that all the field readings are reduced to a datum surface (in this case mean sea level).

The gravity at a point located at a height h, above the mean sea level is given by

$$g_h = \frac{GM}{R^2}\left(1+\frac{h}{R}\right)^{-2} \qquad (2.48)$$

Applying the Binomial expansion for the term $(1+h/R)^{-2}$ and ignoring the higher order terms and taking only the first two terms gives

$$g_h = \frac{GM}{R^2}\left(1-\frac{2h}{R}\right) \qquad (2.49)$$

The free air correction is therefore given by

$$dg_{FA} = g - g_h = \frac{2gh}{R} = 0.3086h(mgal/m) \qquad (2.50)$$

The free air correction dg_{FA} is added to the gravity reading when the station is above the reference datum and subtracted when it is below.

Bouguer Correction

The correction takes in to account the excess mass of rock between the station and the reference datum, or the mass deficiency that has been ignored in the free air. If there is additional rock between the station and the datum, this will exert a downward attractive force, thus increasing the gravitational acceleration reading at the station.

The mass excess or deficiency is approximated as a flat slab of uniform density. Therefore, the gravity attraction for a point on the surface for such slab is obtained by the following expression:

$$dg_B = 2\pi G\rho h(mgal) \tag{2.51}$$

Where h is the height above/below the datum plane (in m), and ρ is the density of the rock between the station and datum plane. The density value is usually taken as the average density for crustal rocks, which is 2.67gm/m^3.

The bouguer correction is:

- Subtracted if the station is above the datum plane
- Added if the station is below the datum plane

Terrain Correction

The slab correction described previously describes the gravitational variations caused by gentle topographic variations (those that can be approximated by the slab). But it does not adequately address the effect of surface irregularities such as hills (excess mass), above and, valleys (mass deficiency), below the level of the observation point.

Terrain correction is done by computing graphically the gravity effects at the observation point of all hills above the station level and all valleys below it. A systematic methodology for performing this task was formalized by Sigmond Hammer in 1939.

The terrain corrections require the use of a chart known as graticule as well as a good quality of topographic maps (~10m contour interval or better) of the survey area. Then the correction is computed by dividing the terrain in to vertical columns using concentric circles of different radii drawn at suitable angular intervals.

For such arrangement the correction term is given as

$$dg_{TC} = G\rho\phi\left[r_2 - r_1 + \left(r_1^{\,2} + z^2\right)^{1/2} - \left(r^2{}_2 + z^2\right)^{1/2} \right](mgal) \tag{2.52}$$

where, T is terrain factor

ρ is density

ϕ is angular interval for sectors, [rad]

r_1, r_2 are inner and outer radii of the sectors respectively and

z in the mean elevation

Both topographic features affect the gravity measurement in the same sense, which is reducing the reading due to upward attraction by the excess mass of hills or mass deficiency due to valleys. Therefore, terrain corrections are always positive.

2.2.5 Gravity Anomalies

Any local deviation of gravity from what is normally expected as regular or smooth trend is a gravity anomaly. Such anomaly is the final output of the data processing from which geological interpretations are made. In general free air anomaly gives information about the actual gravity information along the surface of the earth; while bouguer anomaly gives information about hidden underground masses.

Free Air Corrected Gravity (Δg_{FA})

The free air correction accounts for gravity variations resulted from elevation differences in the observation locations. Here the attraction of materials between the station and the reference ellipsoid will not be taken into consideration. Because of this, the variation is known as free air anomaly. Thus, this free air anomaly is given as

$$\Delta g_{FA} = g_{obs} - \left(g_N - 0.3086h\right)\left(mgal\right) \tag{2.53}$$

where g_{obs} = Drift corrected observed gravity

g_N = Normal gravity

h = Elevation (in meters)

Bouguer Slab Corrected Gravity (Δg_B)

The bouguer correction is a first order correction to account for excess mass underlying the observation datum plane. It also accounts for mass deficiency at observation points that is located below the datum plane (sea level).

The bouguer anomaly is the difference between measured gravity value at the station and the theoretical gravity value calculated for that elevation. The form of the bouguer anomaly after ignoring the topographic effect is known as simple bouguer anomaly and is given by:

$$\Delta g_B = g_{obs} - \left(g_N - 0.3086h + 0.0419\rho h\right)\left(mgal\right) \tag{2.54}$$

Terrain Corrected Bouguer Gravity (Δg_{TC})

The terrain correction accounts for variations in the observed gravitational acceleration caused by variations in topography near each station. The terrain correction is positive regardless of whether the local topography consists of a hill or valley. The form of terrain corrected bouguer anomaly is known as complete bouguer anomaly and is expressed as

$$\Delta g_{TC} = \Delta g_B + dg_{TC}\left(mgal\right) \tag{2.55}$$

where dg_{RC} is the value of the computed terrain correction (2.52).

Assuming all the corrections made for the measured gravity have accurately accounted for the variations in gravitational acceleration they have intended to account for, any remaining variations in the gravitational acceleration associated with the complete bouguer gravity can now be caused by geologic structures.

Density Variations of Earth Materials

Density is diagnostic parameters in the gravitational methods of exploration and the small anomalies, sought in this method, are generally related to the local variations in it.

Comparing to other geophysical parameters such as: magnetic susceptibility, electrical conductivity and others, the density variation of Earth materials is very small.

We can notice from the table below that the relative variation in rock density is quite small, which is about 0.8gm/cm^3, and there is considerable overlap in the measured densities. Hence, knowledge of rock density alone will not be sufficient to determine rock type. The small variation in rock density also implies that the spatial variations in the observed gravitational acceleration caused by geologic structures will be quite small and thus difficult to detect.

Table 2.1 The density of various Earth materials.

Material	Density (g/cm^3)
Air	~0
Water	1
Gravel	1.7-2.4
Sandstone	1.61-2.76
Shale	1.77-3.2
Limestone	1.93-2.9
Granite	2.5-2.81
Basalts	2.7-3.3
Metamorphic Rock	2.6-3.3

difference (usually referred as density contrast) between the ore body and the surrounding soil. That is, the special variation in the gravitational acceleration generated would be exactly the same if we were to assume different densities for the ore body and the surrounding soil, as long as the density contrast, $(\rho_2 - \rho_1)$ were kept constant.

2.2.6 Local and Regional Gravity Anomalies

In addiction to the types of gravity anomalies defined on the amount of processing performed to isolate geological contributions, there are also specific gravity anomaly types defined on the nature of the geological contribution.

There are two contributions to our observed gravitational acceleration. The first is caused by large-scale geologic structure that is not of interest. The gravitational acceleration produced by these large-scale features is referred to as the Regional Gravity Anomaly. The second contribution is caused by smaller scale structure for which the survey was designed to detect. That portion of the observed gravitational acceleration associated with these structures is referred to as the Local or Residual Gravity Anomaly. Because the Regional Gravity Anomaly is often much larger in size that the Local Gravity Anomaly, it is imperative that we develop a means to effectively remove this effect from our gravity observations before attempting to interpret the gravity observations for local geologic structure.

Separating Local and Regional Gravity Anomalies

Because Regional Anomalies vary slowly along a particular profile and Local Anomalies vary more rapidly, any method that can identify and isolate slowly varying portions of the gravity field can be used to separate Regional and Local Gravity Anomalies. The methods generally fall into three broad categories:

- **Direct Estimates -** These are estimates of the regional gravity anomaly determined from an independent data set. Using these observations, we can determine how the long wavelength gravity field varies around our survey and then we can remove its contribution from our data
- **Graphical Estimates** – These estimates are based on simply plotting the observations, sketching the interpreter's estimate of the regional gravity anomaly, and subtracting the regional anomaly estimate from the raw observations to generate an estimate of the local gravity anomaly.
- **Mathematical Estimates** – These represent any of a wide variety of methods for determining the regional gravity contribution from the collected data through the use of mathematical procedures. These includes the following:
    - **Moving Averages** – In this technique, an estimate of the regional gravity anomaly at some point along a profile is determined by averaging the recorded gravity values at several nearby points. Averaging values over several observation points enhances the long wavelength contributions to the recorded gravity field while separating the shorter wavelength contributions.
    - **Function Fitting**– In this technique, smoothly varying mathematical functions are fit to the data and used as estimates of the regional gravity anomaly. The simplest of any number of possible functions that could be fit to the data is a straight line.
    - **Filtering and Upward Contribution** – These are more sophisticated mathematical techniques for determining the long wavelength portion of a data set.

2.2.7 Error Assessment of Gravity Data

The accuracy of the computed gravity anomalies depend on the error introduces while determining different parameters. The random error unavoidable error in the determination of Δg_B for each gravity point arises from the errors involved in the determination of the observed value of g gravity, the pint elevation, the geodetic latitude, the reduction density of the mass between the geoid and at each station. As a result the accuracy, $\sigma\Delta g$ in the determination of point Bouguer anomalies, Δg , is depend on the precision in the determination of g_{obs}, h, g and ϕ . These values are determined independently for each observation point i.e. precession σg_{obs}, σh, $\sigma\phi$ and $\sigma\rho$ in the determination of g, h, ϕ and ρ respectively are uncorrelated. However, it is difficult to asses the error in gravity value due to reduction density in bouguer and terrain corrections.

$$\sigma^2_{\Delta g}=\sigma^2_{g}+(\partial\Delta G_{FA}/\partial h)^2(\sigma_h)^2+(\partial\Delta G_B/\partial h)^2(\sigma_h)^2+(\partial\Delta G\Phi/\partial\Phi)^2(\sigma\Phi)^2+(\partial\Delta G\rho/\partial\rho)^2(\sigma\rho)^2 \qquad (2.56)$$

Twelve independent observations made at four stations located, at Science Faculty, Langano and Shala. The precision in the process of measuring the relative value, $\sigma g_{obs,}$ can be evaluated by computing the internal variance (Hammer, 1973) of the n independent observations at m station using equation (2.57)

$$\sigma^2 g = \frac{\sum_{i=1}^{m}(VV)}{n-m} \qquad (2.57)$$

Where m is the number of cheek point and $c_{i\ ,}$ the i th cheek point, and V are residuals for the individual observation at each cheek point. In this particular study the value of n and m are 12 and 4 respectively. As a result the measurement precision, σ g, is evaluated using the outlined results in table (3.1) and the formula.

$$\sigma^2 g = \frac{\sum_{c_1}(vv)+\sum_{c_2}(vv)+\sum_{c_3}(vv)\sum_{c_4}(vv)}{8} \qquad (2.57)$$

Table 2.2 Observed relative gravity value (m) for computing the internal variance of independent observation taken at four check point.

station	g_{obs}	$\hat{g}_{obs}$	V	VV	$\sum_{C_1}(VV)$
	1680.05	1680.057	-0.002	0.00004	0.0001089
C1	1680.050	1680.057	-0.007	0.000049	
	1680.065	1680.057	0.008	0.000064	
	1802.227	1802.097	0.13	0.0169	0.03307
C2	1801.97	1802.097	-0.127	0.01613	
	1802.095	1802.097	-0.002	0.00004	
	1803.658	1803.8	-0.142	0.02064	0.033829
C3	1803.91	1803.8	0.11	0.0121	
	1803.833	1803.8	0.033	0.001089	
	1800.003	1800.114	-0.111	0.012321	0.020393
C4	1800.14	1800.114	0.026	0.000676	
	1800.2	1800.114	0.086	0.007396	

$$\sigma g = \pm\left|\frac{0.0001089 + 0.03307 + 0.033829 + 0.020393}{8}\right|^{1/2} \quad (2.58a)$$

$$\sigma g = \pm 0.104523\text{mGal} \quad (2.58b)$$

This implies one may encounter an error of $\pm$ 0.104523mGal while taking readings with this gravimeter.

The partial derivatives, $\left(\frac{\partial \Delta g_{FA}}{\partial h}\right), \left(\frac{\partial \Delta g_B}{\partial h}\right)$ and $\left(\frac{\partial \Delta g_B}{\partial \phi}\right)$ Can be determined by evaluating the partial derivative of the gravity correction formulas, section 2.2.4 with respect to h, and ϕ respectively hence the second, the three and the fourth terms in equation 2.56 are expressed as follows

$$\left(\frac{\partial \Delta g_{FA}}{\partial h}\right) = 0.3086 mGal/m \quad (2.59a)$$

$$\left(\frac{\partial \Delta g_B}{\partial h}\right) = 0.0419 \rho mGal/m \quad (2.59b)$$

$$\left(\frac{\partial \Delta g_\phi}{\partial \phi}\right) = \frac{1}{R}\left(\frac{\partial g_N}{\partial \phi}\right) = 0.811 \sin(2\phi) mGal/km \quad (2.59c)$$

For Bouguer reduction density of 2.67g/cm^3 and the precision in elevation determination of the altimeter used in the survey area, 3m and for the mean radius R, estimated to be 6371229m, the rate of change of the normal gravity with latitude is given by (2.59c) is found to be about 0.0413mGal for the mean latitude of the study area, $\phi \leq 7.53$ for each meter traveled in the N-S direction.

The overall mean square error of the Bouguer anomaly at each station, Δg_B based on the theory of error propagation determined by the equation (2.56), neglecting the last term in the equation amounts to:

$$\sigma_{\Delta g} = \left[(0.10452^2) + (0.85707^2) + (0.11268^2) + (0.0378^2)\right]^{1/2} = \pm 1.01 mGal$$

This shows that most of the error in gravity values comes from the error in elevation. The accuracy level can be quoted as ±1.5 mGals and in the data processing of the gravity data, two mGal contour interval can be used for reliable result.

2.3 THE MAGNETIC METHOD

Magnetic observation have been successfully employed, not only in the search for magnetic ore, but also in locating buried hills, geological faults, intrusions of igneous rocks, salt domes associated with oil fields, concealed meteorites and buried magnetic objects such as pipe-lines.

2.3.1 Basic concepts and units of Geomagnetism

Around a bar magnet, a magnetic flux exists, as indicated by the flux lines in figure 2.10, and converges near the ends of the magnet, which are known as the magnetic poles. If such a bar magnet is suspended in free air, the magnet will align itself with the earth's magnetic field with one pole (the positive north-seeking) pointing towards the earth's north Pole and the other (the negative south-seeking) towards the south magnetic pole. Magnetic poles always exist in pairs of opposite sense to form a *dipole.* When one pole is sufficiently far removed from the other so that it no longer affects the other, the single pole is referred to as a *monopole.*

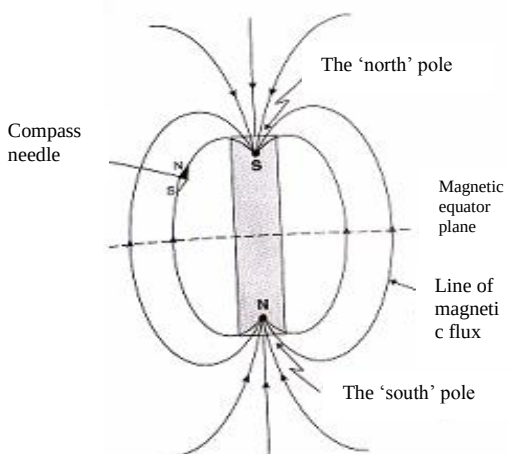

Figure 2.9 Lines of magnetic flux around a bar magnet.

If two magnetic poles of strength p_1 and p_2 are separated by a distance r, a *force F* exists between them (2.56). If the poles are of the same sort, the force will push the poles apart, and if they are of opposite polarity, the force is attractive and will draw the poles towards each other. Note the similarity of the form of the expression in 2.56 with that for the force of gravitational attraction in (2.31); both gravity and magnetism are potential fields and can be described by comparable potential field theory.

$$F = \frac{p_1 p_2}{\mu r^2} \tag{2.60}$$

where μ is a constant of proportionality known as the *magnetic permeability*,

p_1 and p_2 are the strengths of the two magnetic monopoles, and

r is the distance between the two poles.

The constant, μ , depends upon the magnetic properties of the medium in which the poles are situated. This force is attractive, if the poles are different in sign, and repulsive in they are of like in sign.

A more practical quantity than the force is the strength of the magnetic field existing at a point in space, as a result of a pole strength p1 located at a distance r from it. The magnetic field strength H is defined as the force per unit pole:

$$H = \frac{F}{p_2} = \frac{p_1}{\mu r^2} \tag{2.61}$$

The poles of a magnet exist in pairs and they referred as dipoles. The magnetic moment M of a dipole with strength p and a distance L apart given by

$$M = pL \tag{2.61}$$

The magnetic moment is a vector in the direction of a unit vector extending from the negative pole towards the positive pole.

When a magnetic material is placed within a magnetic field strength, *H*, the magnetic material will produce its own magnetization. This phenomenon is called *induced magnetization*. In practice, the induced magnetic field will look like it is being created by a series of magnetic dipoles located within the magnetic material and oriented parallel to the direction of the inducing field, *H*. The strength of the magnetic field induced by the magnetic material due to the inducing field is called the intensity of magnetization, I.

The intensity of magnetization defined as the dipole moment per unit volume V of a material, given by

$$I = \frac{M}{V} \tag{2.63}$$

The intensity of magnetization, *I*, is related to the strength of the inducing Magnetic field, *H*, through a constant of proportionality, *k*, known as the Magnetic Susceptibility, which is a measure of how susceptible a material is to becoming magnetized.

$$k = \frac{I}{H} \tag{2.64}$$

The magnetic susceptibility is a unit less constant that is determined by the physical properties of the magnetic material. It can take on either positive or negative values. Positive values imply that the induced magnetic field, *I*, is in the same direction as the inducing field, *H*. Negative values imply that the induced magnetic field is in the opposite direction as the inducing field.

In magnetic prospecting, the susceptibility is the fundamental material property whose spatial distribution we are attempting to determine. In this sense, magnetic susceptibility is analogous to density in gravity surveying.

The ratio of the flux density **B** (also called *magnetic induction*) to the magnetizing field strength H is a constant called the *absolute magnetic permeability* (μ). Practically, the magnetic permeability of water and air can be taken to be equal to the magnetic permeability of free space (vacuum), denoted by μ_0 which has the value of $4\mu x10^{-7} Wb/Am$. For any medium other than a vacuum, the ratio of the permeabilities of a medium to that of free space is equal to the *relative permeability* μ_r, such that $\mu_r = \mu/\mu_o$ and, as it is a ratio, it has no unit.

$$B = \mu H \tag{2.65}$$

Since $\mu = \mu_r \mu_o$ the above equation be comes

$$B = \mu_r \mu_o H \tag{2.66}$$

Rearranging to introduce $k = \mu_r - 1$ and we have

$$B = \mu_o H + \mu_o kH = \mu_o (H + I) \tag{2.67}$$

Where H and I are in the same direction, as is usually the case. The SI unit for **B** is the tesla=1newton/ amper-meter=1weber/meter^2(Wb/m^2). In vacuum $\mu_r = 1$ and in air $\mu_r \approx 1$. In magnetic prospecting, we measure **B** to about 10^{-4} of the earth's main field. The unit of magnetic induction generally used for geophysical work in the nanotesla (also called the gamma, γ) in which $1\gamma = 10^{-9} T = 1nT$.

2.3.2 Magnetism of the earth

As far as exploration geophysics is concerned we can separate the earth's magnetic field in to the following three parts:

1. The *main magnetic field,* which is produced in the core of the earth and accounts for the very large regional variations in the field intensity and direction.
2. The *external magnetic field,* which is produced by electric currents in the earth's ionosphere consisting of particles ionized by solar radiation and put into motion by the solar tidal force.
3. The *anomalous magnetic field,* which is produced by ferromagnetic minerals in the earth's crust.

Mathematically we can write the above as follow

$$B_T = B_{ext} + B_{\text{int}er} = B_{ext} + B_D + B_{rm} \qquad (2.68)$$

where B_T = the total magnetic field.

B_{ext} = External magnetic field

B_D = Dipole field, which is generated by the fluid outer core.

B_{rm} = The field of rock magnetism

2.3.3 Origin of geomagnetic field

The earth acts like a huge bar magnet in which its magnetic field on its surface and in the space around it varies. According to Sir William Gilbert the geomagnetic field originates from a giant bar magnet (dipole) located at the center of the earth and its axis inclined 11.5^0 from the earth's axis of rotation.

Although, such a bar magnet fits the magnetic field on the surface of the earth, its origin was questionable. Experiment showed that any magnet loses its magnetization at a temperature greater than 500^0C, which is known as Curie's temperature. In addition the outer core is at a molten state and the temperature at the inner core is about 4200^0C. Hence such a magnet proposed by Gilbert actually does not exist at the center of the earth.

After the rejection of Gilbert's proposal, several hypotheses have been raised. Nowadays the accepted hypothesis among the several is: *the self exited dynamo theory.* This theory is base on the idea that the geomagnetic field originates from the coupled fluid motions and electric currents in the liquid outer core.

2.3.4 Time Varying Magnetic Field

In the early days of navigation with the compass, it was recognized that the earth's magnetic intensity changes its direction slowly and irregularly. Later measurements at magnetic observatories showed many

changes in the field that have shorter periods than those originally observed. The variations may be resolved into secular changes, solar-diurnal changes, lunar diurnal changes and changes resulting from magnetic storms.

Secular Variation: - Slow changes in the earth's field which take place progressively over decades or centuries are known as secular variations. Such changes are noted in the world.

Diurnal Variation: - The most direct significance in magnetic prospecting are the smaller but more rapid oscillations in the earth's field which have a periodicity of about a day and amplitude is averaging about 25 gammas. Diurnal variations are regularly recorded at magnetic observatories. The records generally show two types of variations, the quite day and the disturbed day. The quite day variation is smooth, regular, and low in amplitude: it can be separated in to predictable components having both solar and lunar periodicities. The disturbed day variation in less regular and is associated with magnetic storms.

On magnetically quite days analysis of magnetic observatories records shows a definite 24-h periodicity that depends, to a close approximation, only on local time and geographic latitude. Because of its correlation with the period of the earth's rotation as referred to the sun, this portion of the variation is referred to as the *solar-diurnal variation*. The average range of this variation in magnetic intensity is of the order of 30 gammas.

Another component in the periodic variation of the earth's magnetic elements has about one-fifteenth the amplitude of the solar-diurnal variation and a periodicity of approximately 25-h corresponding to the length of the lunar day. This component of the variation has been related to the earth's rotation with respect to the moon and is referred to as *lunar-diurnal variation.* Its low amplitude makes it less important as a source of disturbance in magnetic prospecting that the solar component.

Magnetic Storms: - In addition to the predictable short-term variations in the earth's field, there are transient disturbances, which by analogy with their metrological counterparts are called *magnetic storms.* Such storms cause considerable disruption in magnetic prospecting operations. The oscillations that take place while they are going on are so rapid and unpredictable that it usually is not feasible to correct for them as with diurnal variations. Magnetic surveys must generally be discontinued during storms of any severity. From the equator to latitude of 60^0, the oscillations during such storms may have amplitude as great as 1000 gammas.

2.3.5 Diamagnetism, Paramagnetism and Ferromagnetism

All atoms have a magnetic moment as a result of the orbital motion of electrons around the nucleus and the spin of the electrons. According to quantum theory, two electrons can exist in the same electron shell

(or state) as long as they spin in opposite directions. The magnetic moments of two such electrons, called *pair electrons,* will cancel out. In the majority of substances, when there is no external applied magnetic field, the spin magnetic moments of adjacent atoms are distributed randomly so there is no overall magnetization. In a *diamagnetic* material, such as halite, all the electron shells are completely filled so there are no unpaired electrons. When an external magnetic field is applied, a magnetization is induced. The electrons orbit in such away so as to produce a magnetic field that opposes the applied field giving rise to a weak, negative susceptibility.

Unpaired electrons in incomplete electron shells produce unbalanced spin magnetic moments and weak magnetic interactions between atoms in *paramagnetic* materials such as fayerite, amphiboles,olivines, garnets and biotite. In an external applied field, the spin magnetic moments align themselves into the same direction, although this process is retarded by thermal agitation. The result is a weak positive susceptibility according to the Curie-Weiss Law. Paramagnetism is generally at least an order of magnitude stronger than diamagnetism.

In *ferromagnetic* materials, the susceptibility is large but is dependent upon temperature and the strength of the applied magnetic field. The spin moments of unpaired electrons are coupled magnetically due to the very strong interaction between adjacent atoms and overlap of electron orbits. A small grain in which magnetic coupling occurs forms what is called a *single magnetic domain* and has dimensions of the order of micron. This gives rise to a strong 'spontaneous magnetization' that can exist even when there is no external applied field. The magnetic coupling can be such that the magnetic moments are aligned either parallel or antiparallel.

Truly ferromagnetic materials occur only rarely in nature but include substances such as cobalt, nickel, and iron, all of which have parallel alignments. Ferromagnetism disappears when the temperature of the material is raised above the *Curie temperature* T_C, as inter-atomic magnetical coupling is severely restricted and the material thereafter exhibits paramagnetic behavior. In *antiferromagnetic* material, for example hematite, the moments are aligned in an antiparallel manner. Although the magnetic fields of the oppositely oriented dipoles cancel each other out, crystal lattice defects result in anet residual moment or *parasitic (anti)-ferromagnetism.* In ferrimagnetic materials, of which magnetite, titanomagnetite and ilmenite are prime examples, the sub-lattices are unequal and antiparallel. This results in a net magnetization. Spontaneous magnetization and large susceptibilities are characteristics of ferrimagnetic materials, such as in the case of pyrrhotite. Although the temperature dependence of ferrimagnetic behavior is complex, ferrimagnetism disappears at temperatures above the Curie point. The majority of naturally occurring magnetic materials exhibit either ferrimagnetic or imperfectly antiferromagnetic characteristics.

2.3.6 The earth's magnetic elements

A vector is used to represent the earth's magnetic field at an observation site. This vector is described by a combination of seven quantities we call the *magnetic elements*. They are illustrated in figure 2.11. Magnetic *declination, d,* is the angle between geographical north and the direction of north that is indicated by a compass. *Inclination, i,* is the angle between the field direction and a horizontal plane. The total field intensity F can be separated into a vertical component Z and a horizontal component H in the magnetic north direction. That horizontal component can be separated into an intensity component X in the geographical north direction and an intensity component Y in the geographical east direction. These seven magnetic elements are related in the following ways

$$\left.\begin{aligned} F^2 &= H^2 + Z^2 = X^2 + Y^2 + Z^2 \\ F &= \frac{H}{\cos i} = \frac{Z}{\sin i} \\ \cos d &= \frac{X}{H} \\ \sin d &= \frac{Y}{H} \end{aligned}\right\} \quad \text{Magnetic north} \qquad (2.69)$$

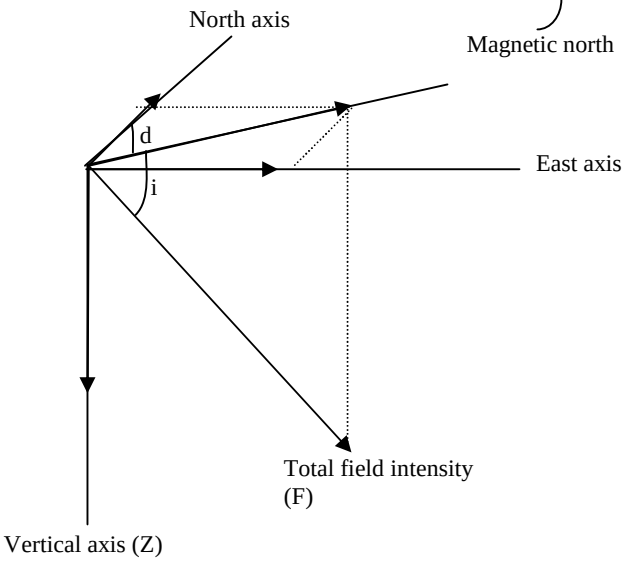

Figure 2.10: The elements of magnetic field.

2.3.7 Noise and Corrections for Magnetic Variations

All magnetic data sets contain elements of noise and will require some form of correction to the raw data to remove all contributions to the observed magnetic field other than those caused by sub-surface magnetic

sources. In ground magnetometer surveys, it is always advisable to keep any magnetic objects (keys, penknives, some wristwatches, etc), which may cause magnetic noise, away from the sensor. It is also essential to keep the sensor away from obviously magnetic objects such as cars, metal sheds, power lines, metal pipes, electrified railway lines, walls made of maffic rocks, etc.

There are several ways of correcting magnetic data according to the various magnetic variations. For the secular variation of magnetic data a model is known as International Geomagnetic Reference Field (IGRF) has been prepared from comparison of individual magnetic responses in different areas of magnetic observatories. So, it has become standard processing practice for magnetic survey that the applicable IGRF (updated to the time of the survey) is subtracted from the observed values of the total magnetic intensity.

The most significant correction is for the diurnal variation in the Earth's magnetic field. The necessary corrections are mostly attempted by the reoccupation of the base station which is located in or near the survey area.

Variations in magnetic field due to magnetic storms can be so rapid, unpredictable, and of such large amplitude, that normally no corrections can be made. Magnetic surveying is therefore generally discontinued under these conditions.

CHAPTER THREE

DATA ACQUISITION, PROCESSING AND PRESENTATION

3.1 The Resistivity Method

3.1.1 Field Procedure and Data Acquisition

The schlumberger array is mostly used in vertical electrical sounding for its better depth penetration and that it is less sensitive for lateral inhomogeneities because the potential electrodes remain fixed during a number of successive measurements with expanding current electrodes.

For this study the symmetrical schlumberger array which is the vertical electrical sounding (VES) was conducted along three lines which are about 2.5km apart. The VES were carried out with maximum current electrode spacing (AB/2) of 500m by injecting electrical current in to the ground by means of two outer electrodes, and the resulting potential difference were measured by a second pair of potential electrodes placed near the center of the outer electrodes (figure 2.6).

A total of nine vertical electrical soundings (VES) were taken so as to understand the subsurface conditions of the study area. Each lines contains three VES, in which, all lines are oriented in NW-SE direction (figure 3.1). The VES was done at an average interval of 450m. The current electrode spacing selected for these surveys were AB/2(in meter): 1.5, 2.1, 3.0, 4.2, 6.0, 9.0, 13.5, 20.0, 30.0, 45.0, 66.0, 100.0, 150.0, 220.0, 330.0 and 500.0 and the potential electrodes spacing were MN/2(in meter): 1.0, 12.0 and 90.0. The overlap readings were taken at AB/2: 20.0, 30.0, 150.0 and 220.0m in order to avoid the ambiguity of inhomogeneity.

The basic equipment required for the electrical resistivity survey consists of a transmitter, a receiver, steel electrodes, electrical cables and connectors. The instruments used as transmitter and receiver are: PASI 16GL earth resistivity meter and P100 energizer DC source respectively.

The table given below shows the GPS coordinates and the elevations which was recorded during the electrical resistivity survey for each of the VES points.

Table 3.1 The GPS location and elevation of the VES points.

VES number	UTM (m)		Elevation(m)	Remark
	Easting(E)	Northing(N)		
VES1-1	464744	832412	1607	On line 1
VES1-2	645057	832031	1605	On line 1
VES1-3	465658	831484	1602	On line 1
VES2-1	464034	829536	1649	On line 2
VES2-2	464293	829399	1648	On line 2
VES2-3	464667	829228	1646	On line 2
VES3-1	462515	827530	1705	On line 3
VES3-2	462872	827182	1703	On line 3
VES3-3	463057	826952	1702	On line 3

3.1.2 Data Reduction

The apparent resistivity values are plotted on logarithmic transparent paper. In processing of the collected data, the apparent resistivity values were written on the ordinate and the electrode separation (AB/2) on the abscissa. The resistivity measurements were made by progressively increasing the potential electrode distance (MN/2) relatively large increment of the current electrode distance (AB/2). In most cases the sounding curve is segmented due to overlap measurement and can not be interpreted as it is. To have precise interpretations the segmented curves were shifted to the small MN curve points, so that the effect could be quantified and corrections could be made in order to obtain a single smooth curve that could be processed with the computer software known as 'RESIST87'.

3.1.3 Data Processing and Presentation

The Schlumberger sounding data collected in the field were interpreted by using two layer master curves and auxiliary charts to obtain the true layer resistivities and thickness. The layer parameters obtained from the curve matching process were used as starting model in the RESIST87 inversion program which resulted in improved best fitting parameters. Due to the availability of borehole lithological logs (Table 1.1), on the preceding chapter one, around the study area it was possible to constrain the final models so that the results become geologically plausible.

The VES data were plotted on a bi-logarithmic graph paper of modules 62.5mm. The preliminary interpretation was done using practical curve matching technique using two layer master curve and auxiliary point charts. The layer parameters obtained by this technique were used as initial model parameters for the inversion done by the computer program RESIST87. The program has an option to fix some model

parameters from the well known sources and has iteration. The iteration for this study was performed to determine true depth and true resistivity values of the ground and minimize the ambiguity from the equivalency problem. The sounding curves were obtained with RMS error of less than 5%.

The layer parameters acquired by the RESIST87 program were used to construct geoelectricsections for each line (traverse) to show the subsurface conditions using the software AutoCAD2008.

The field data have been plotted along each line by the help of "SURFER" to get pseudosections using the apparent resistivity and pseudo depth values (AB/2) and these plots represent the overall resistivity picture on a vertical section. These pseudosections could help us to get a generalized picture of the sub surface of the area and check for the consistency of the results.

3.2 THE GRAVITY AND MAGNETIC METHODS

3.2.1 Field Procedures and Data Acquisition

In geophysical exploration gravity and magnetic methods are mostly used side by sides. In the gravity method the variation of the earth's gravitational field is interpreted as a subsurface mass distribution in terms of geological structures. The method is useful in locating dense intrusion, rift structures like faults, graben and horsts. Magnetic method is routinely employed for subsurface study to outline structural lineaments which could be associated with faults and fractures that may serve as conduits for groundwater.

Gravity and magnetic surveys were carried out on three different traverses which are approximately 2.5km apart. These traverses are on the same lines as that of the VES points as can be seen in the figure 3.1. The gravity survey was conducted using CG3 gravimeter. It has a reading accuracy of 0.05mgal. The positions of the survey stations were determined using the GPS receiver, Garmin 12, and the station elevations were measured using altimeter MM-1.

The secondary gravity base station located at Bekele Mola hotel was used to tie each station gravity readings with the gravity base net of the country. Each day gravity data reading was started and ended up at this base station. At each station the gravimeter reading, recording time, its location in UTM coordinate and elevation (meter) were recorded.

In our magnetic survey a Scintrex made proton precession magnetometer, IGS-2, was used by selecting the option for total field mode. This mode has an operating range of 20000 to 100000 nT. It has an absolute accuracy of $\pm$2nT at 100000nT and 1nT accuracy at 50000nT. It has a 2 sec reading times with a resolution

of 0.1nT. Tuning field could be selected either manually or can be made automatic using a keypad, for this survey the automatic tuning was selected.

The routine magnetic data collection was started and ended by taking base station readings situated around each line. Hence we have three base stations, for the first line BS1 located at a UTM coordinate 464240easting and 833054northing, for the second line BS2 at 464143easting and 829483northing and the third one BS3 at the position of 462884easting and 827177northing.

At each station the magnetometer reading, recording time and its location in UTM coordinate were recorded. During the measurement the magnetometer was mounted on a back harness and is oriented in such a way that the "equatorial region up" arrow imprinted on it points as required by the geographic location of the survey area and also measurements were made always facing to one direction, towards north, that is the direction of the ambient field. A tuning field of 35,500 nT was selected.

Data were collected along the three traverse lines at approximate stations interval of 50m for magnetometer readings and 100m for gravimeter reading.

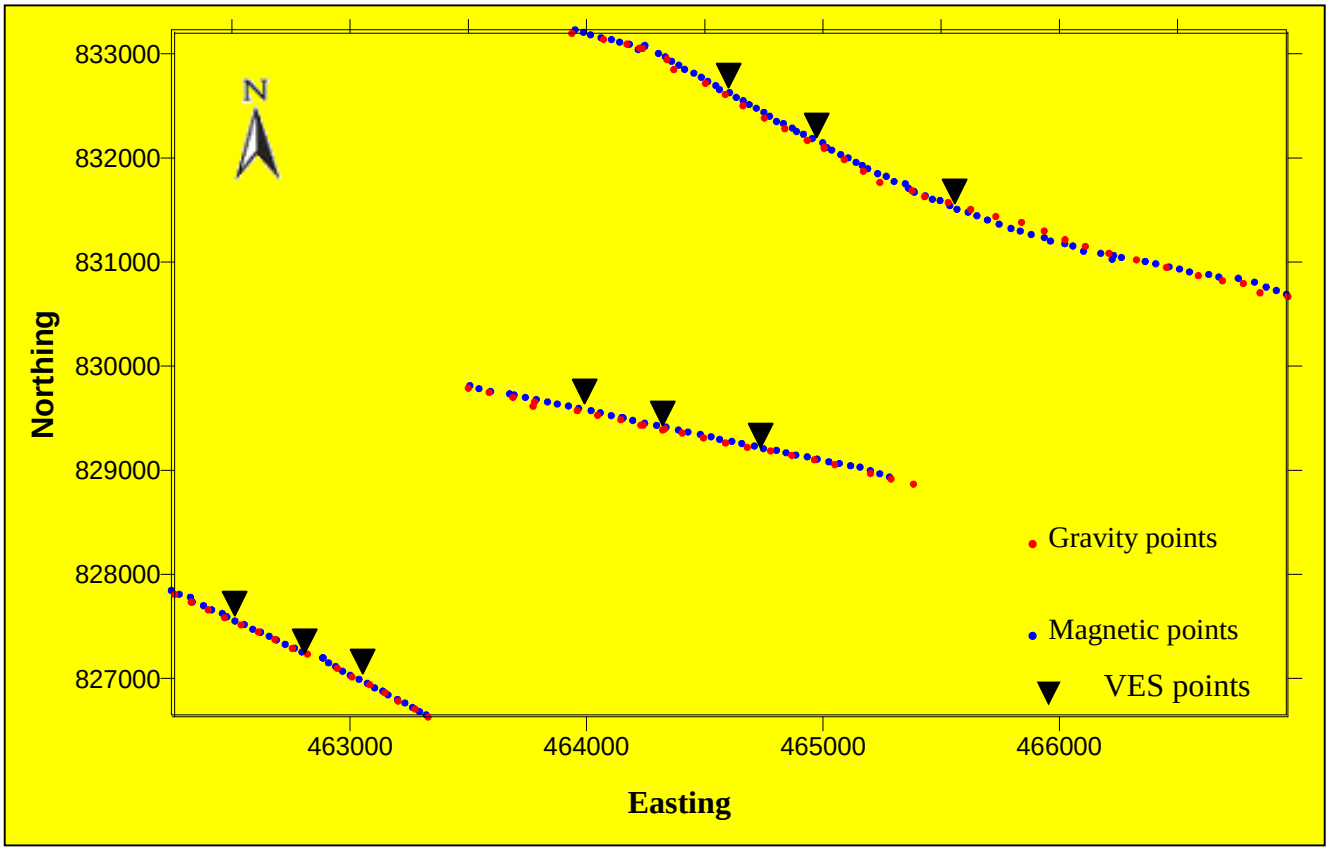

Figure 3.1 Locations of data points.

3.2.2 Data Processing and Presentation

At the very beginning it is very important to establish base station before the start of gravity survey. This base station must be tied to the international gravity net with respect to IGSN71. For this study the primary base of the Addis Ababa Geophysical Observatory with absolute gravity value of 977452.16 mgal is found to be appropriate to prepare our temporary (secondary) base station at Bekele Mola hotel. The value of the observed gravity for our base station is found to be 977584.5mgal. The gravimeter surveys which are carried out along the three lines are tied with respect to the base station at Bekele Mola so as to complete the loop as well as for the computation of the gravity reductions.

When we come to Magnetometer survey, before establishing base stations around each line the first thing that was done is to look for appropriate location with very less magnetic noises such as cars, houses with iron roof and others. For this study the base stations for each line were reoccupied within one hour interval for the correction of diurnal variation.

For both gravimeter and magnetometer data which were collected on the survey site, the standard "GEOSOFT" computer program were employed. 'Gravred' which is DOS based program was used to obtain all gravity outputs such as: simple bouguer anomaly, free air anomaly, latitude and longitude after providing all the necessary inputs such as date, elevations, coordinates, average density, reference datum(IGRF 1967), raw gravity readings and others which were required by the program.

To produce different maps for both potential methods 'MAGMAP' were found to be very important. All the maps are presented on figure 4.10, figure 4.11, figure 4.12 and figure 4.13 as free air anomaly, elevation, simple bouguer anomaly and residual high pass maps respectively for the gravimeter data. Where as figure 4.14 and figure 4.15 are prepared as total magnetic field map and analytical maps and for the upward continued maps figure 4.16 and figure 4.17 are presented.

Figure 4.18 and Figure 4.19 present the two-modeled section, which were generated with the GM-SYS and MapInfo-8 softwares.

3.2.3 Interpolation

In this study the linear interpolation technique is used to prepare the maps. Interpolation, in general, assigns values to points that have originally no measured data values, depending on the selected searching radius and grid cell. Interpolation is a must, since it is not possible to take infinite measurements that represent the infinite points on the earth's surface. The linear interpolation, in this study, gives gravity and magnetic values for areas covered between the traverse lines (i.e. between the two lakes). Despite its importance, interpolation also has some serious problems when it is used improperly. In order to minimize this problem a searching radius of 500m was used.

CHAPTER FOUR

RESULT AND INTERPRETATIONS

4.1 RESULT AND INTERPRETATION OF RESISTIVITY DATA

4.1.1 Along Line 1

A. Pseudo section along line 1

The generalized electrical feature is shown in figure 4.1. According to this figure the top soil between VES-11 and VES-12 shows high resistivity zone. Low resistivity zones are observed at the bottom of each VES. Much less resistivity can also been seen beneath VES-12.

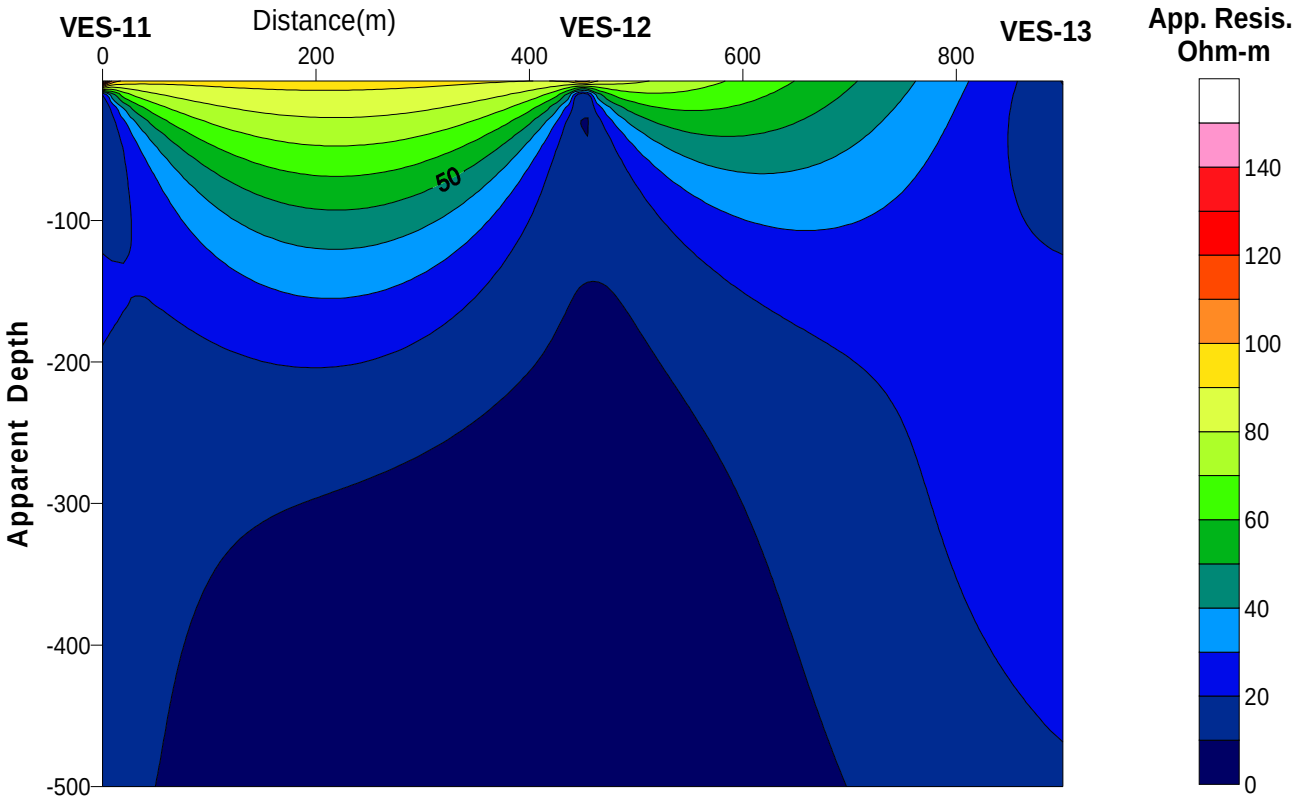

Figure 4.1 Pseudo section along line 1, Langano.

B. Geoelectric section along line 1

From the interpreted layer parameters of VES-11 to VES-13 (Figure 4.2), the resistivity sounding geoelectric section along line 1 is constructed (Figure 4.3). The dry soil is characterized by relatively high resistivity values as well as very resistivity and this difference is believed to be due to variation of moisture content. This layer has nearly 0.9 to 1.8m thickness over the first two VES points. Here the top layer on figure 4.3 is somehow exaggerated.

The second layer form a resistivity range of 7-24Ohm-m and thickness varying 25-31m beneath the VES points. This layer is inferred as fractured ignimbrite. The next layer has 36-72Ohm-m resistivity ranging

which represents weathered ignimbrite. This layer has a thickness of about 19m beneath VES-12 and about 51m and 65m beneath VES-11 and VES-12 respectively.

The last part of the cross section along line 1 is covered by fluid saturated highly fractured ignimbrite having resistivity of 3-12Ohm-m. This low resistivity zone is believed to be a good means for ground water movement between the two lakes.

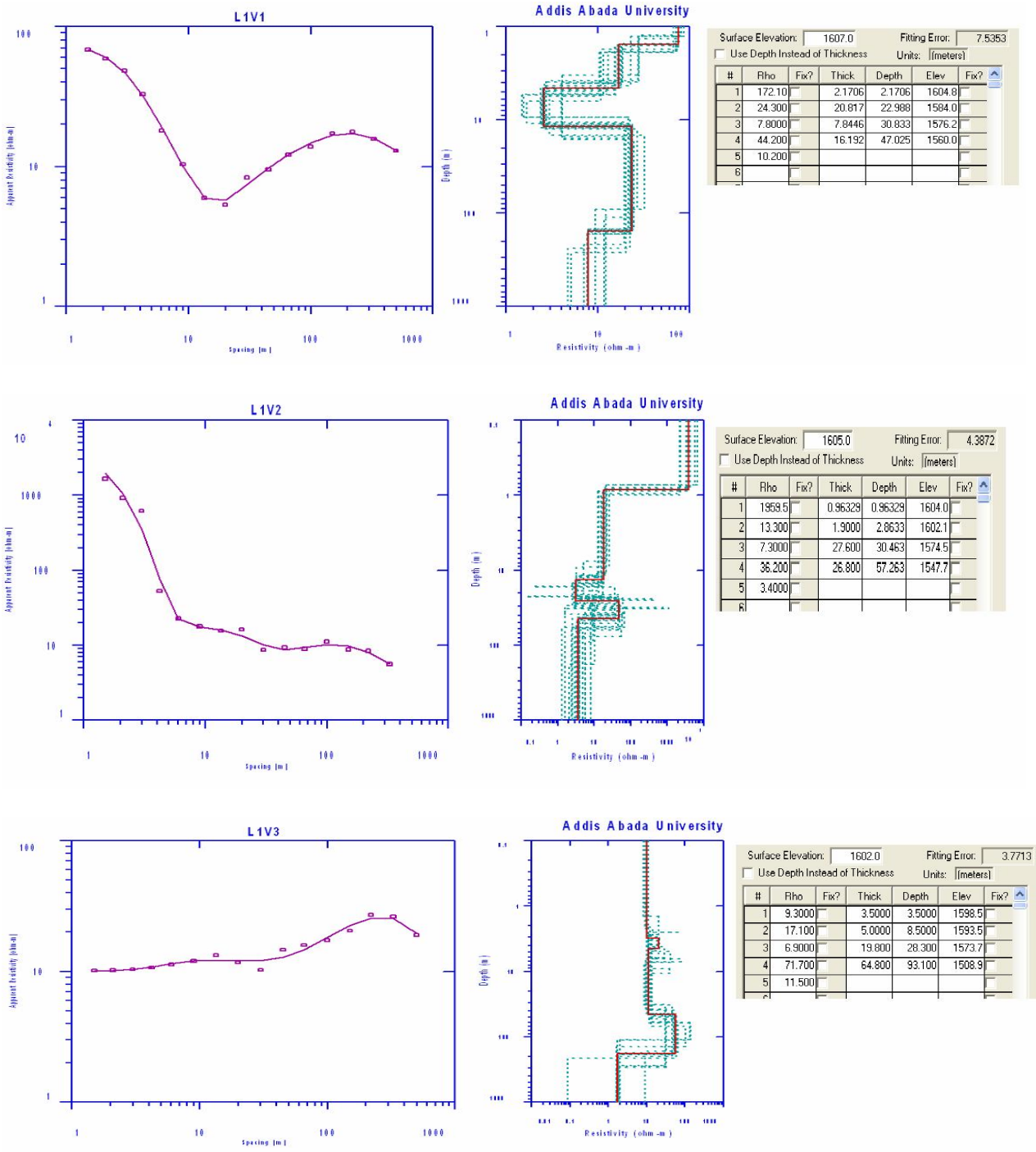

Figure 4.2 Resistivity sounding curves along line 1.

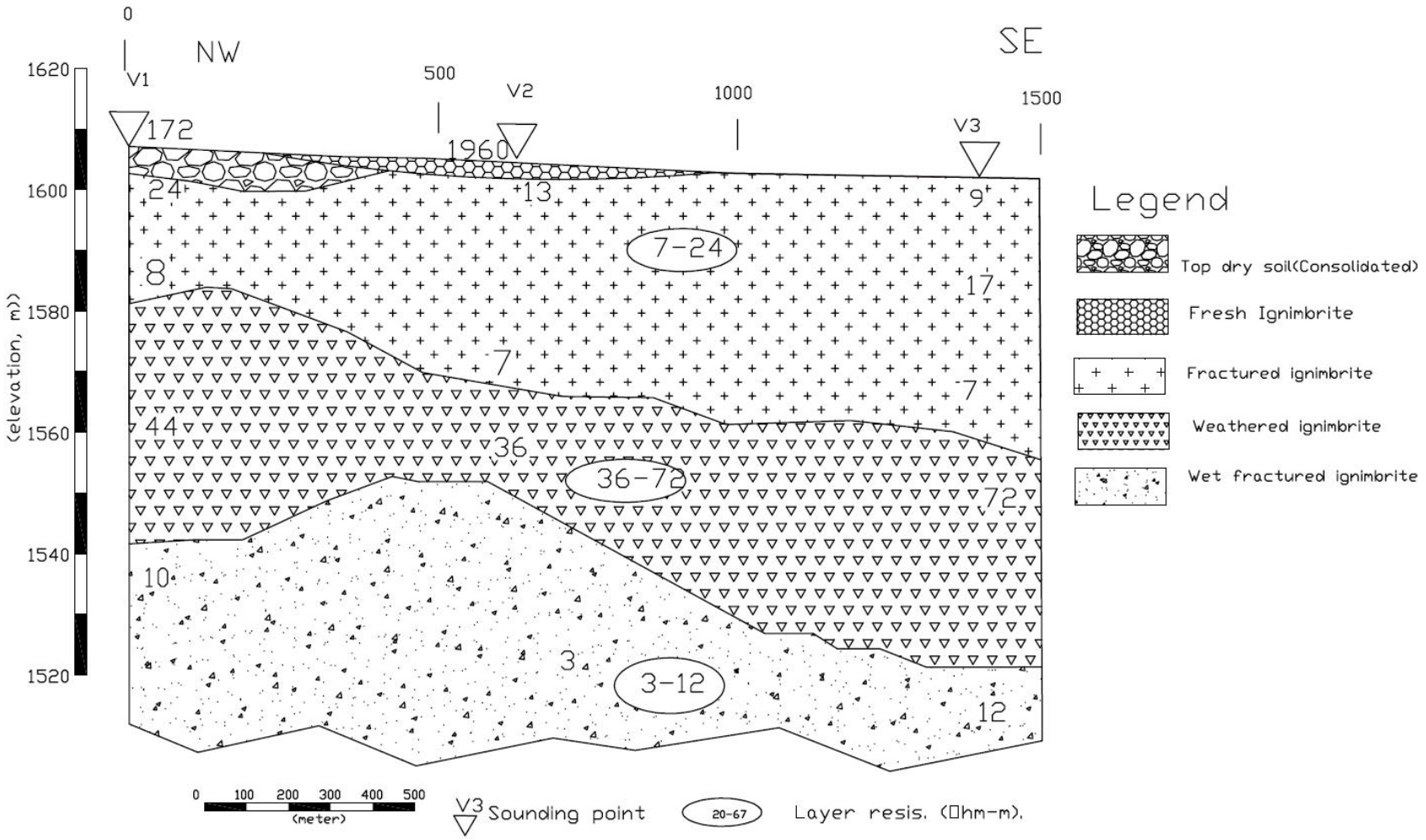

Figure 4.3 : Geoelectric section along Line 1, Langano

4.1.2 Along Line 2

A. Pseudo section along Line 2

Figure 4.4 shows the general electrical picture of the ground section along line 2. High resistivity is observed at the top of VES-23. Resistivities ranging 40-50 Ωm are found below VES-21 and VES-22 and which is also visible below VES-23 at deeper depth. Low resistivity zones, 10-20 Ωm are located at deeper depth beneath VES-21 and VES-22.

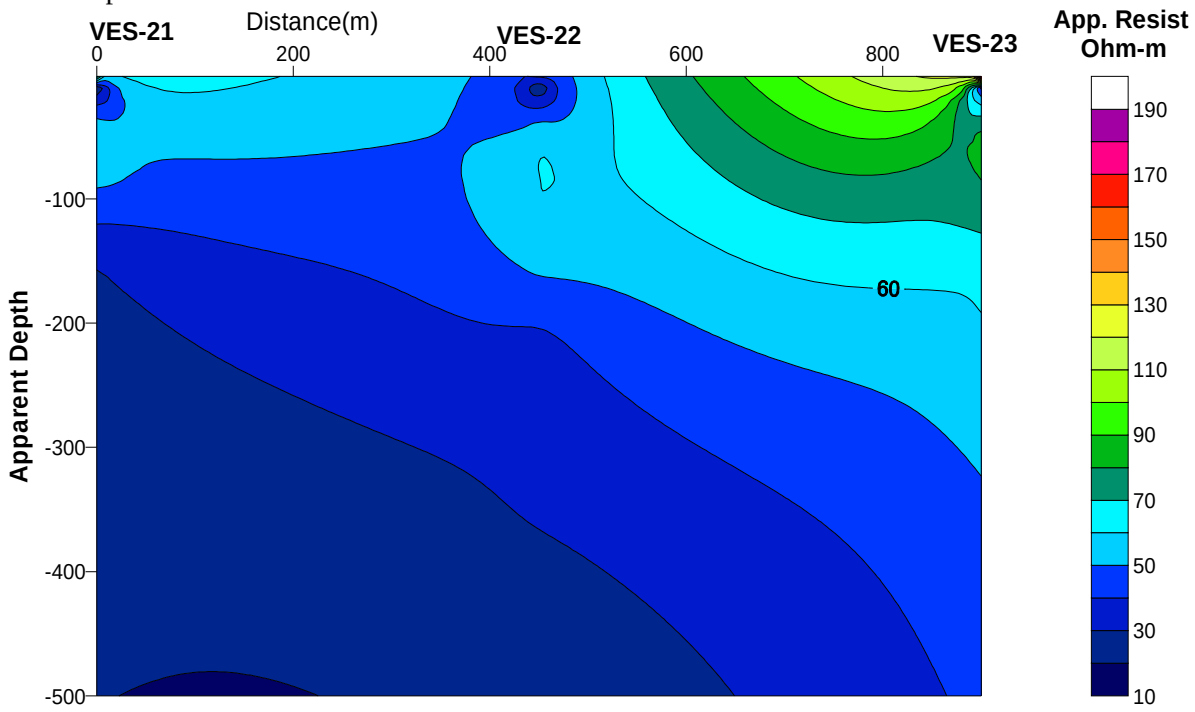

Figure 4.4 Pseudo section along line 2, Langano.

B. Geoelectric section along Line2

From the interpreted layer parameters of VES-21 to VES-23 (Figure 4.5) the resistivity sounding geoelectric section (Figure 4.6) along line 2 is constructed. The resistivity of the upper most layer ranges between 115 to 297 Ohm-m and have thickness 1.1 to 2.1 m. It possibly represents the top dry soil. Here the top layer on figure 4.6 is somehow exaggerated.

Underlying the top layer, beneath VES-21 t0 VES-23, the subsurface is characterized by low resistivity ranging from 5 to 22Ohm-m and has average thickness of 2.3m which represents fluid saturated fractured ignimbrite.

The third and fourth layer beneath VES-21 having resistivity of 4Ohm-m and 350 Ohm-m respectively show large lateral variation in resistivity with respect to the layer beneath VES-22 and VES-23, which has a resistivity range of 77-91Ohm-m.Here the existing resistivity variation possibly shows the presence of contact(?).

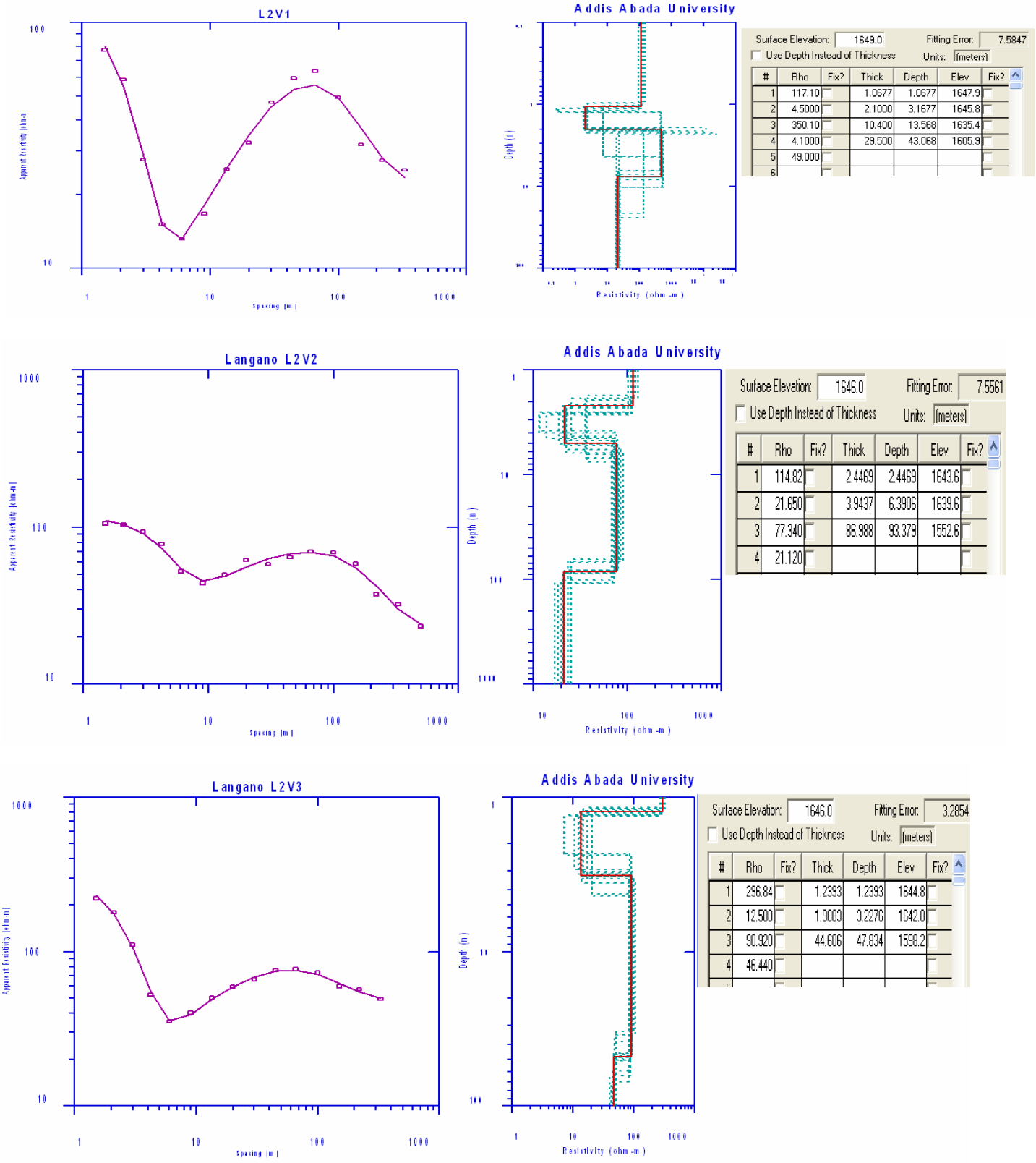

Figure 4.5 Resistivity sounding curves along line 2.

The last layer of the cross section is found below an average depth of 60m.The resistivity varies from 21-49 Ohm-m and it may be attributed to possibly fluid saturated highly fractured ignimbrite which is distributed over the area. This resistivity zone could have from moderate to high permeability for groundwater movement between the two lakes in addition to their elevation difference.

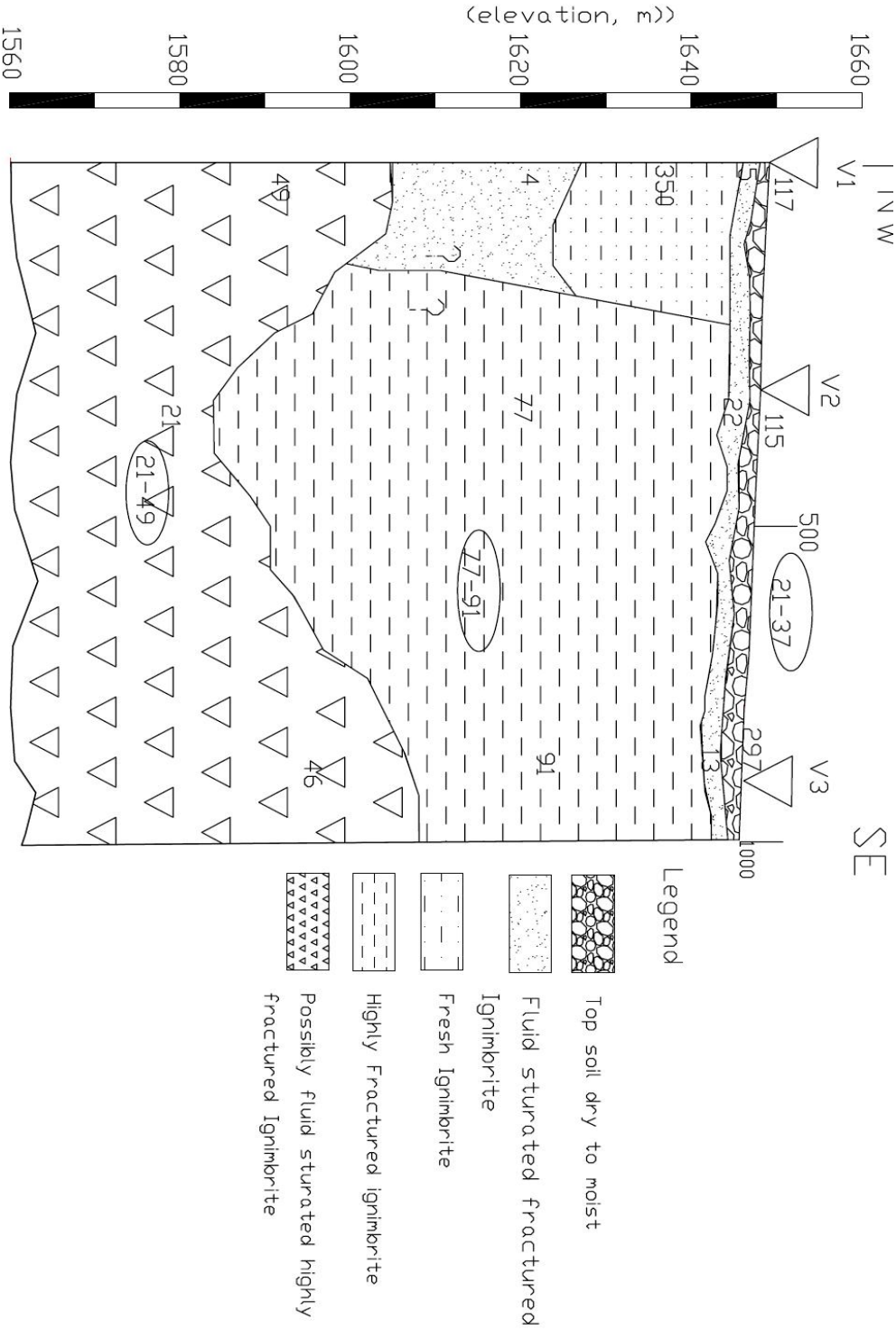

Figure 4.6 : Geoelectric section along Line 2, Langano

4.1.3 Along Line 3

A. Pseudo section along Line3

As the pseudo section of figure 4.7 of this profile shows, the top layer around VES-31 and VES-32 is relatively resistive compared to VES-33. Generally the resistivity decreases with increasing depth. And at deeper depth beneath VES1 and VES2 there exists very low resistivity zone.

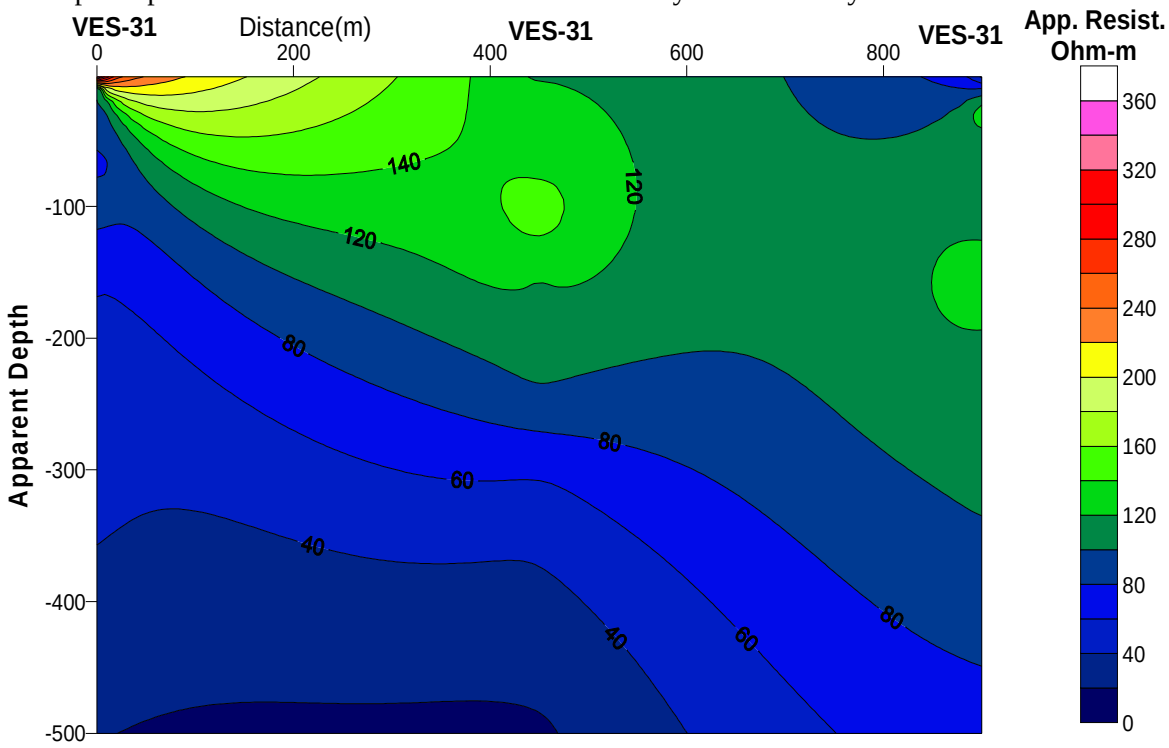

Figure 4.7: Pseudo section along line 3, Langano.

B. Geoelectric section along Line 3

The resistivity sounding geoelectric section along line 3 is constructed from the interpreted layer parameters of VES-31 to VES-33 (figure 4.8). It shows that the area is underlined by different layers beneath each point and the resulting geoelectric section is presented in (figure 4.9). Beneath this line, layers are subdivided laterally by two structures most probably contacts (?).

Figure 4.9 shows, VES-31 and VES-32 have four layers where as VES-33 is consisting of five layers.

The topmost part of the cross section has resistivity values that range from 29 to 319 Ohm-m. This layer is probably related to dry top soil with thickness ranging 0.7m at VES-31 to 1.8m at VES-33. Here the top layer on figure 4.9 is somehow exaggerated.

The second layer below VES-31has resistivity of 836 Ohm-m with thickness 1.1m, below VES-32 there exists massive ignimbrite rock with resistivity 129 Ohm-m having thickness of about 19m and below VES-33, the layer is covered by slightly fractured ignimbrite rock with thickness 2.8m.

The third layer below VES-31 has resistivity of 74 Ohm-m and thickness 117m, informs that the layer is covered by slightly weathered ignimbrite, laterally under VES-32 a layer with thickness 101m and resistivity 150 Ohm-m is identified as massive ignimbrite more over below VES-33 we have highly weathered ignimbrite with resistivity 234 Ohm-m and thickness about 10m.

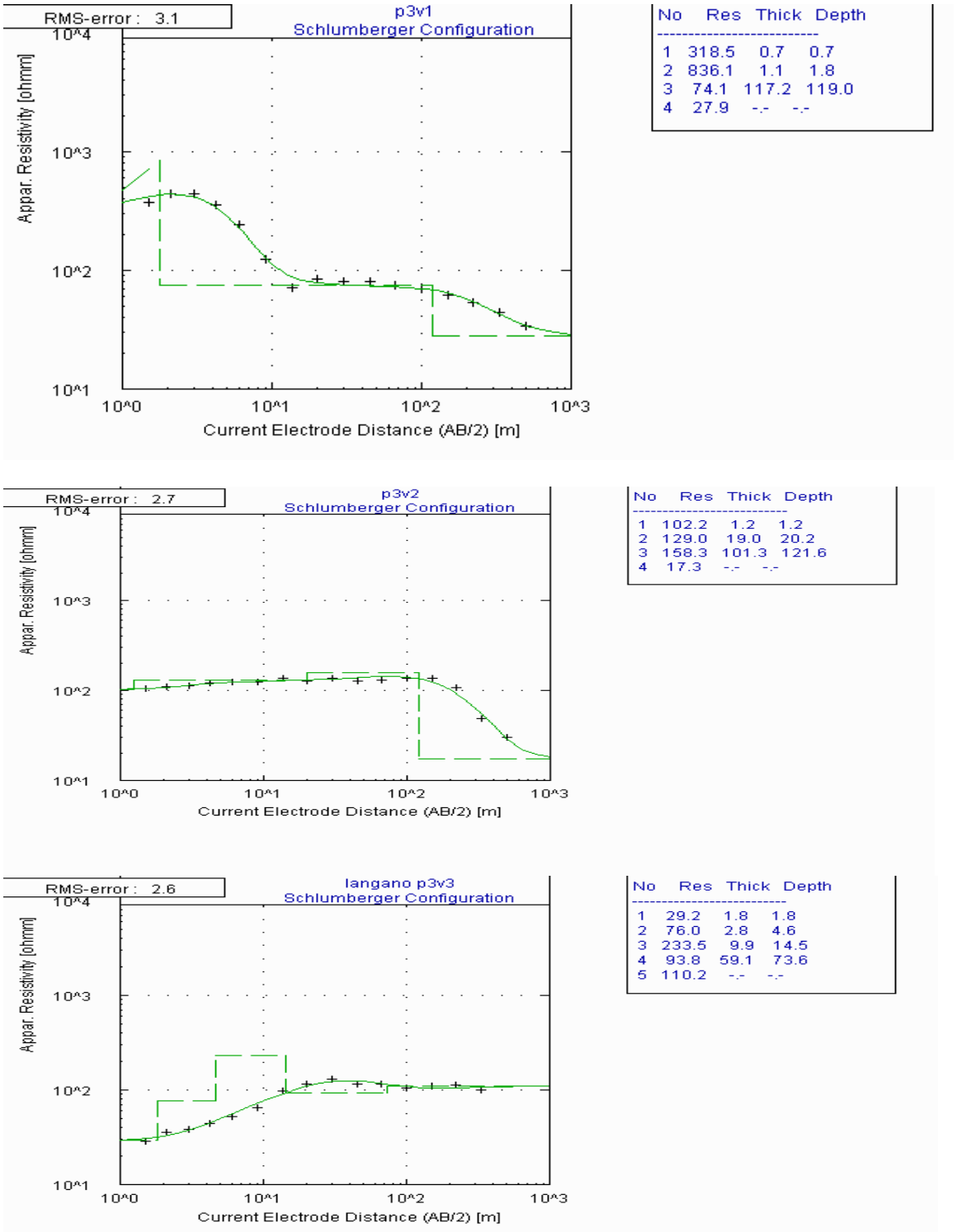

Figure 4.8 Resistivity sounding curves along line 3.

The fourth layer, beneath VES-31 and VES-32, has a resistivity range of 17 to 28 Ohm-m which is at a depth below 100m. This layer could be considered as a good means for conduiting groundwater from Lake Langano towards Lake Shala. The fourth layer under VES-33 has a resistivity 94 ohm-m and thickness 59m followed by fractured massive ignimbrite of resistivity 110 Ohm-m.

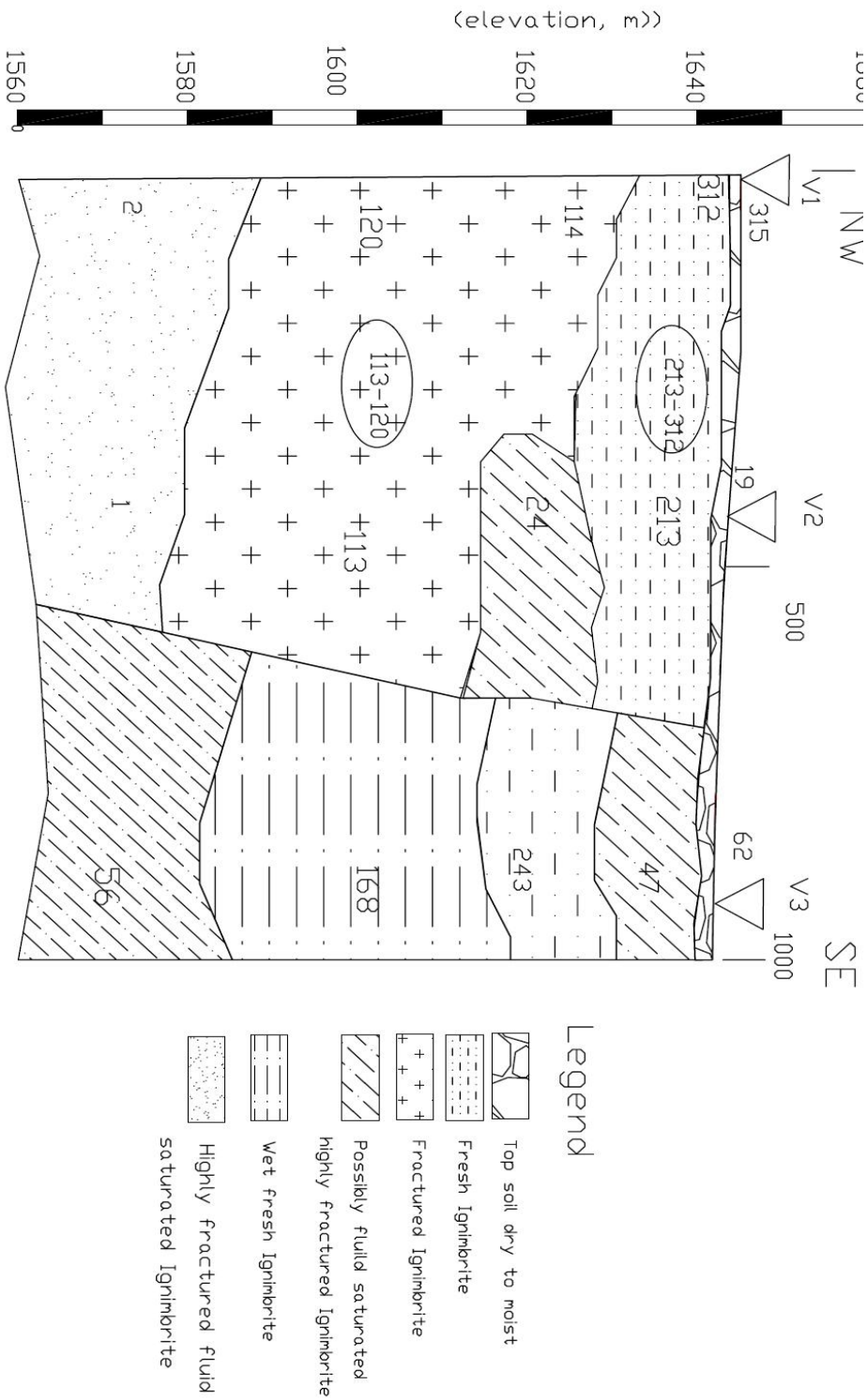

Figure4.9 :Geoelectric section along Line 3, Langano

4.2 RESULT AND INTERPRETATION OF GRAVITY DATA

4.2.1 Free Air Anomaly and Elevation Map

The free air anomaly map of the study area shows a strong positive correlation with the elevation map (figure 4.10 and fig 4.11). The maximum values of elevation and free air anomaly maps are found at the SW of the study area with values 1710m and -20mGal respectively. The minimum values about1579m for the elevation and -50mGal for free air anomaly are observed at NE of the study area. The free air anomaly is produced with a contour interval of 1mGal and this anomaly in general shows the distribution and vertical gradient of the gravity field on the surface of the earth.

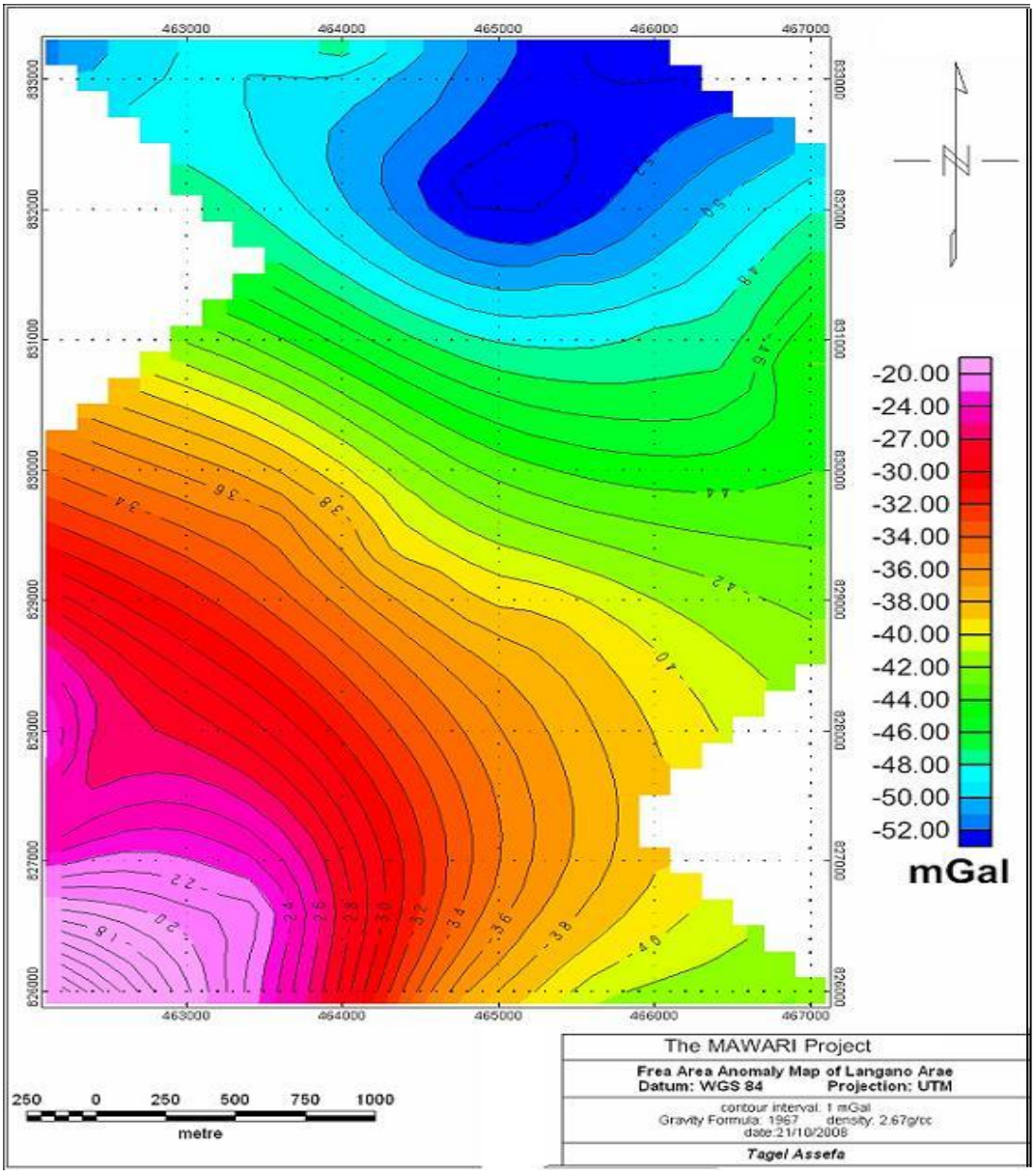

Figure 4.10 Free air anomaly map of the study area.

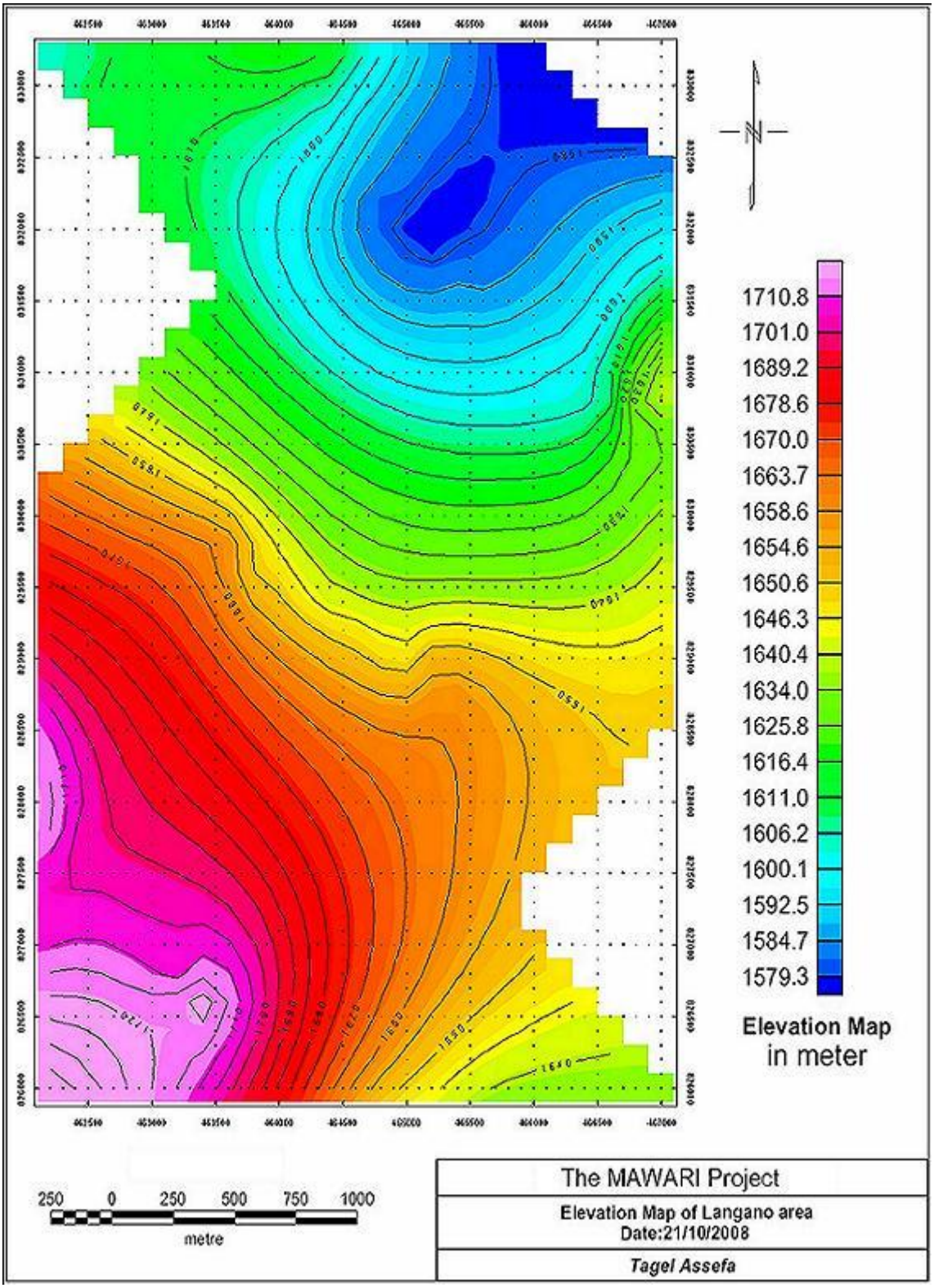

Figure 4.11 Elevation map of the study area.

4.2.2 Simple Bouguer and Residual high pass Anomaly Maps

The bouguer anomaly map in general shows the lateral density variation of the subsurface materials of the earth.

In the bouguer anomaly map of the study area the values range from a minimum -229mGal at the north end of the map where line one is found to wards a maximum value of -212mGal at the SW around line3. This anomaly map is generated with a contour interval of 1mGal (figure 4.12).

The lateral extent of bouguer anomalies due to subsurface anomalous bodies is small as compared with those bouguer anomalies of deep origin anomalous bodies. In general the bouguer anomalies on local scale are caused by the lateral variation in density of subsurface masses. On the other hand the non-homogeneous crust of variable density and thickness causes the anomaly on regional scale.

In all the cases the bouguer anomaly map is the response of both regional and local lithologic units. In order to separate the regional effect from the local anomaly applying different separation technique is very important.

The simple bouguer anomaly map shows low gravity response at relatively low elevated area near SW of lake Langano which could be the result of thick sediment that covers much of the area having somehow low density value. Whereas near NE of lake Shala from the simple bouguer anomaly map we can observe that high gravity response which is probably due to the nearby shala caldera which is the result of denser volcanic rock units.

Residual high pass is one of the filtering techniques used to enhance the effects of smaller geologic units at shallower depth. The effects of shallow masses are usually of short wavelength. The gravity field after near surface noise and the regional effects have been removed is know as residual. To produce the residual high pass anomaly map (figure 4.13) we have used the simple bouguer anomaly result of the study area. Residualizing attempts to remove the regional effect so as to emphasize the residual. However, the separation usually is not complete; both regional and residual are distorted by the effects of each other. Figure 4.13, shows the presence of some short wavelength features at shallower depth between the two lakes.

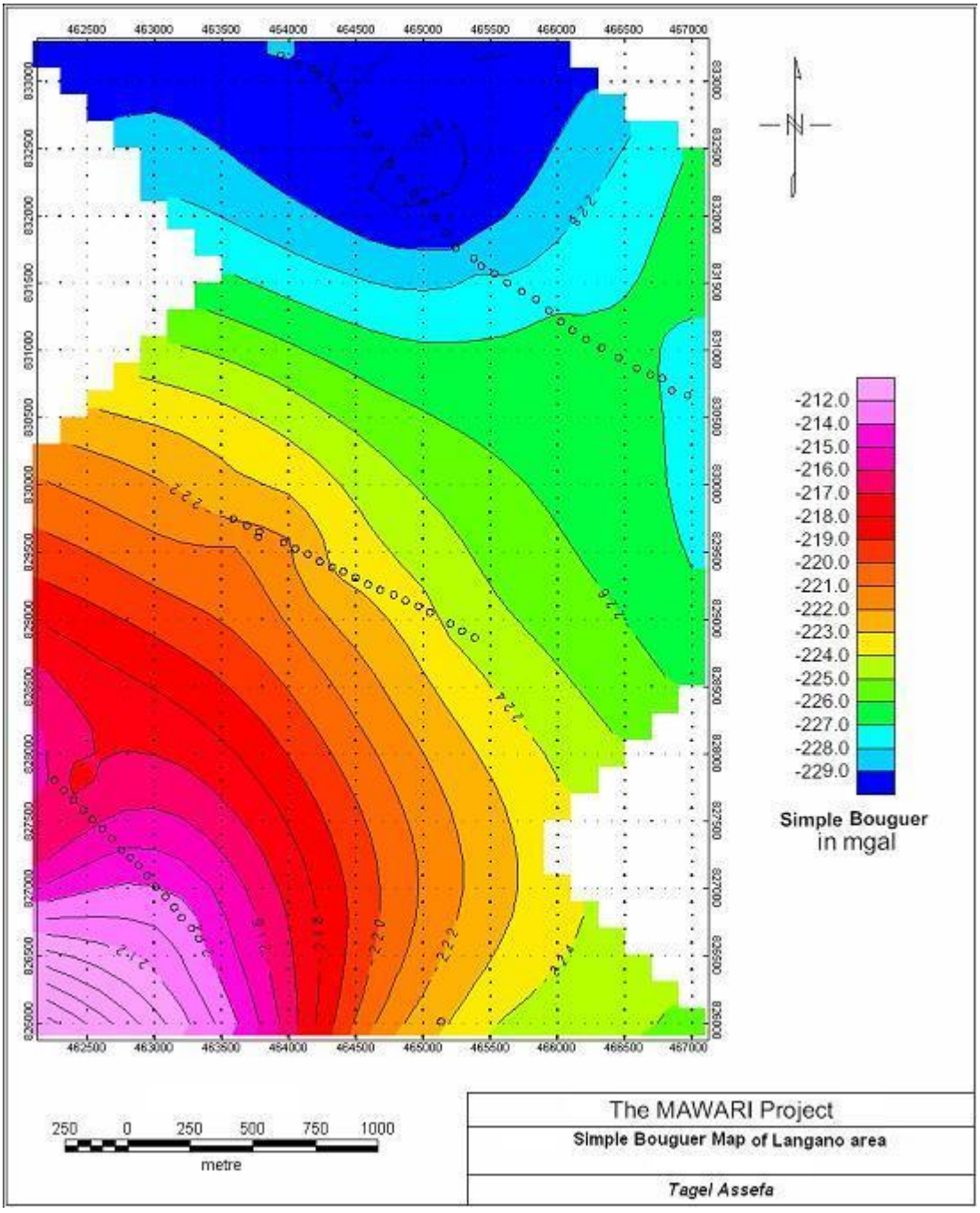

Figure 4.12 Simple Bouguer anomaly map of the study area.

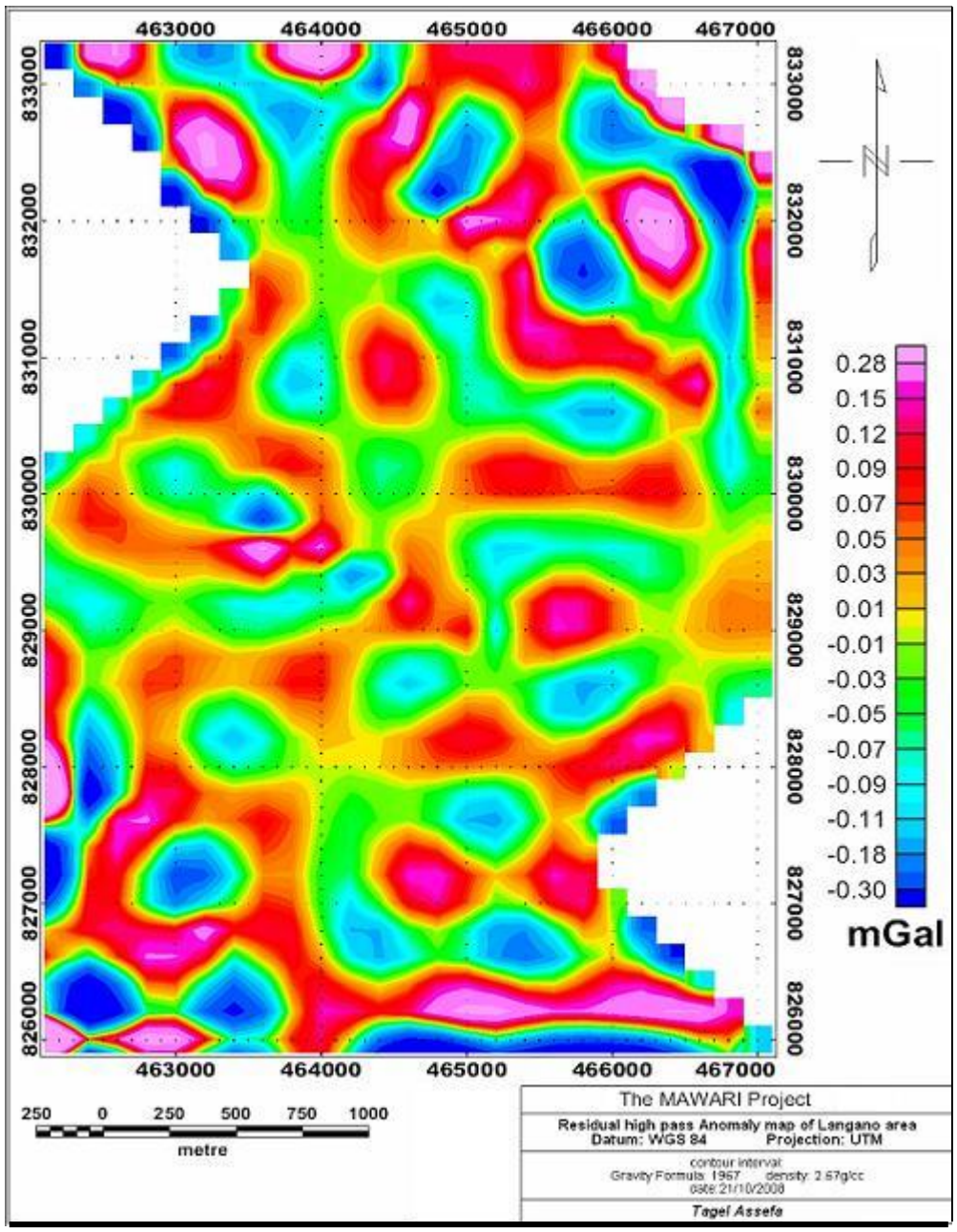

Figure 4.13 Residual High pass anomaly map of the study area.

4.3 Result and Interpretation of Magnetic Data

4.3.1 Total magnetic field anomaly and analytical signal maps

Figure 4.14 represents the total magnetic field anomaly map of the study area. This map shows relatively low magnetic response almost along line 3 as well as from the middle of line 1 to wards the east side of the map. The magnetic high response is observed below the start of line 2 and to wards the west side of the map. This magnetic high response is probably due to the result of highly magnetized volcanic rocks that could be found in the area. Whereas, the low magnetic responses particularly NE of lake Shala, around line 3, could be the result of heat source around the shala caldera. The geological map of the study area also shows the presence of such hot spring at NE of lake Shala.

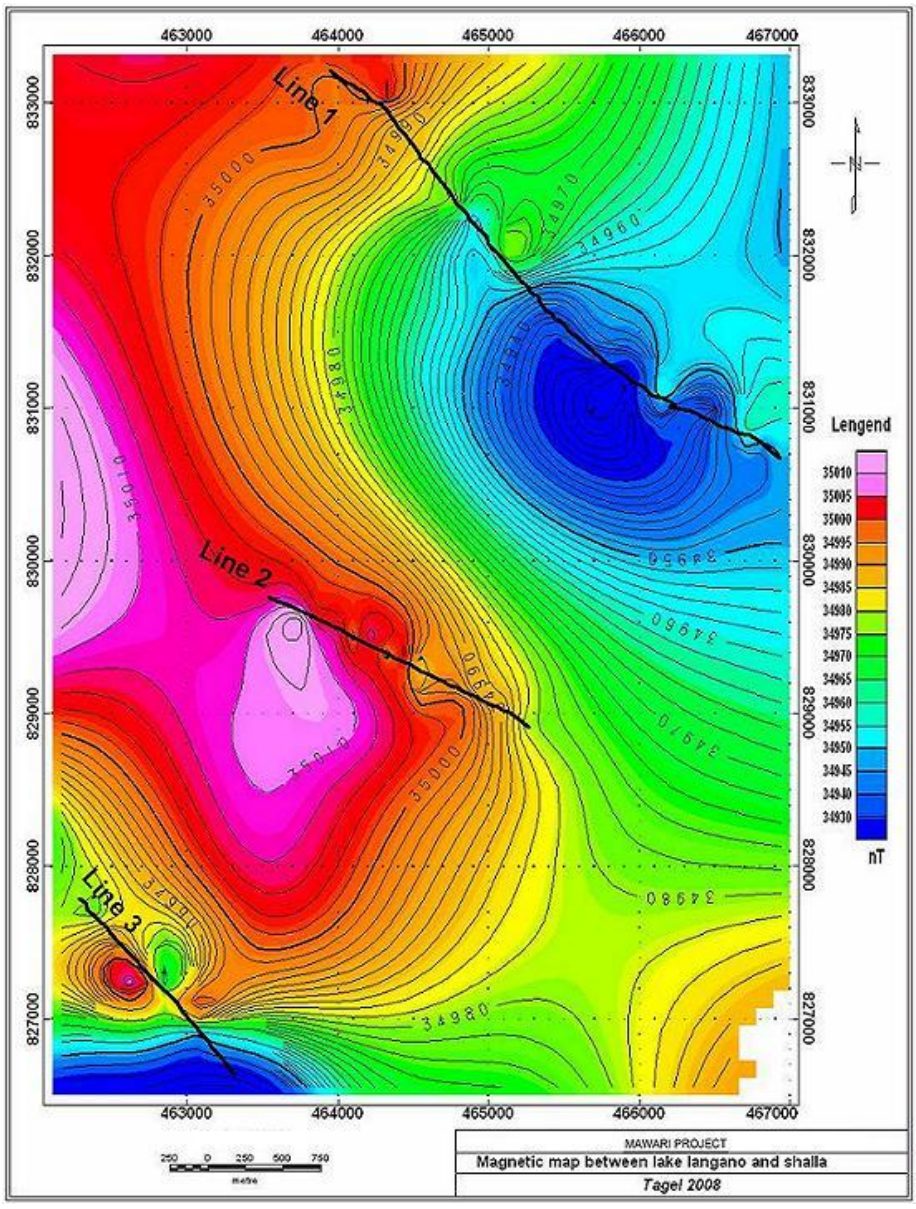

Figure 4.14 Total magnetic field anomaly map of the study area.

The analytical signal is formed through a combination of horizontal and vertical gradients of a magnetic anomaly. The analytic signal has a form over causative bodies that depend on the locations of the bodies but not their directions of magnetization. Furthermore, the map (figure 4.15) shows the responses of anomalous bodies just from the upper part of their sources. This filtering technique might reduce the ambiguity that could rise from the effect of dipole.

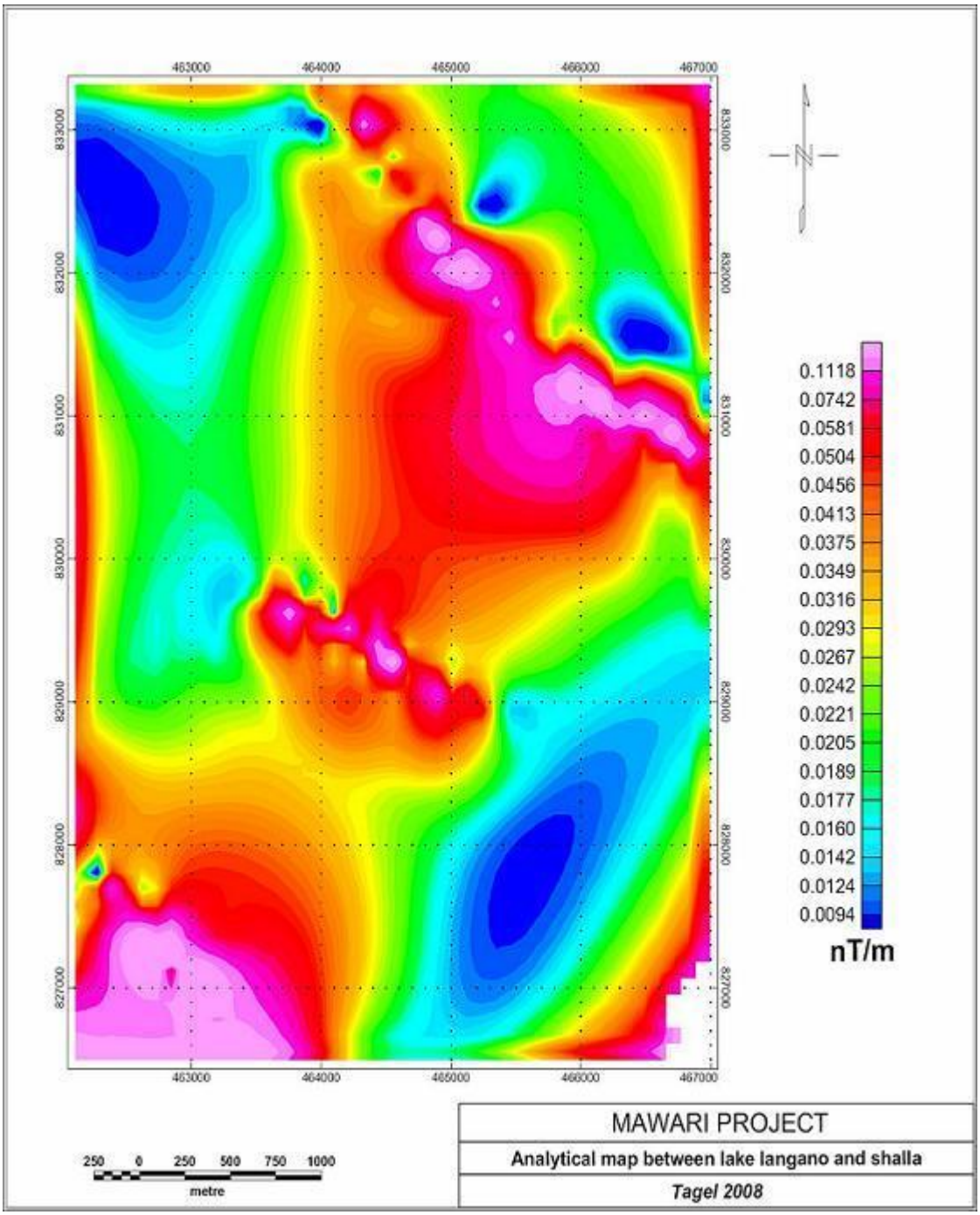

Figure 4.15 Analytical anomaly map of the study area.

4.3.2 Upward continued maps

The effect on the potential field of a geological mass at considerable depth is far less than if it were close to the surface. The principle of continuation is the mathematical projection of potential field data (gravity or magnetic) from one datum vertically upwards or down wards to another datum. Effectively, the continuation process simulates the anomaly at levels below or above sea level as if the data had been obtained at those levels.

Upward continuation is relatively straight forward as the projection is usually into free space. Upward continuation serves to filter out the shorter wavelength anomalies and reduce their amplitudes and decrease noise.

Figure 4.16 and figure 4.17 show the upward continuation maps of the magnetic field up to 100m and 200m respectively. These maps were prepared with the help of GEOSOFT.

The upward continued map (up to 100m) shows the irregular shape anomalies observed on the total magnetic anomaly map become smoothed. The upward continued map (up to 200m) also indicates the low magnetic anomaly observed on the south-west (NE of lake Shala) of the total magnetic anomaly map is enhanced which supports the presence of the source of heat around the area. Generally low magnetic anomaly originated from deeper horizon is observed along south-west and north-east of the study area.

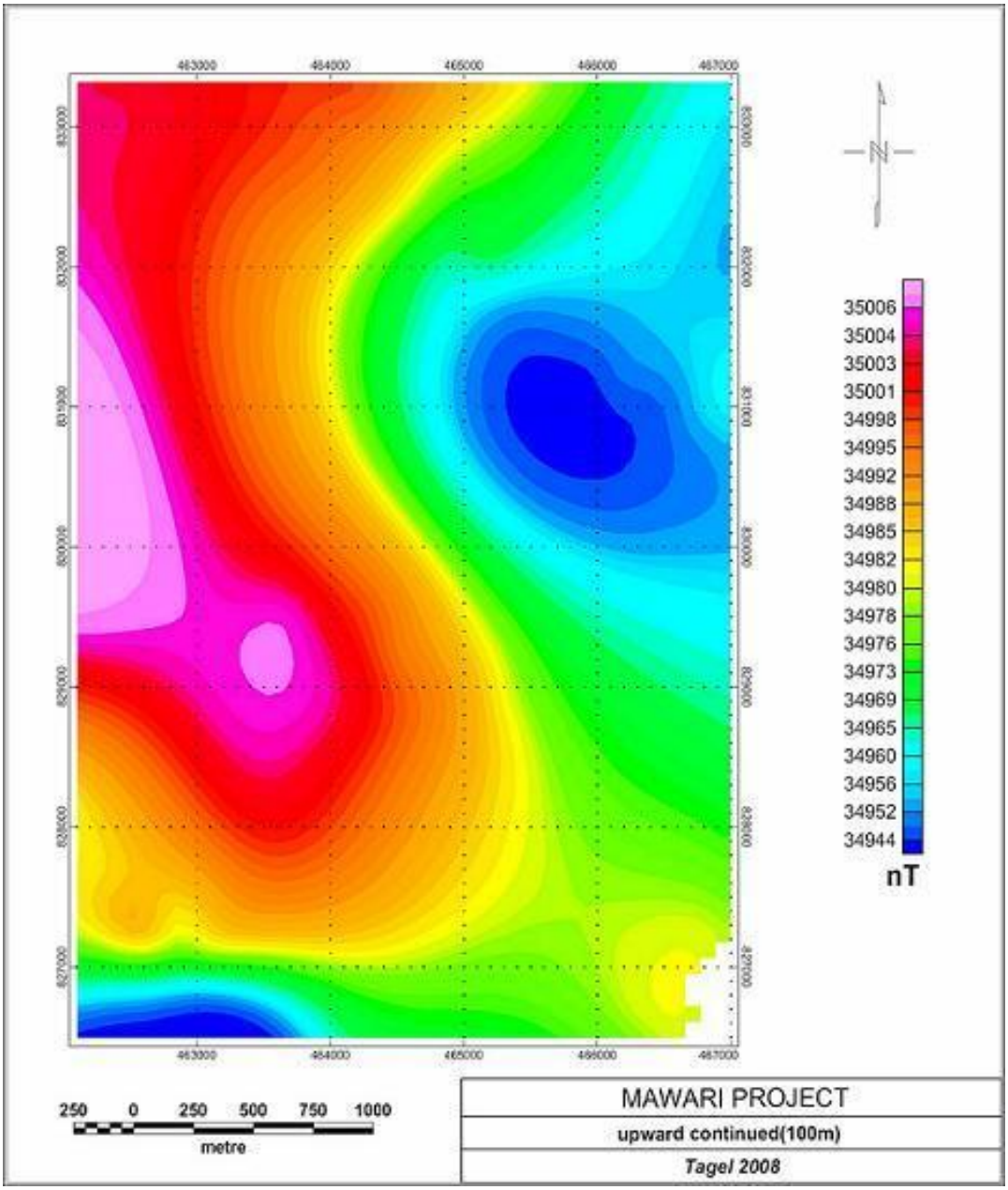

Figure 4.16 Upward continued (up to 100m) map of the study area.

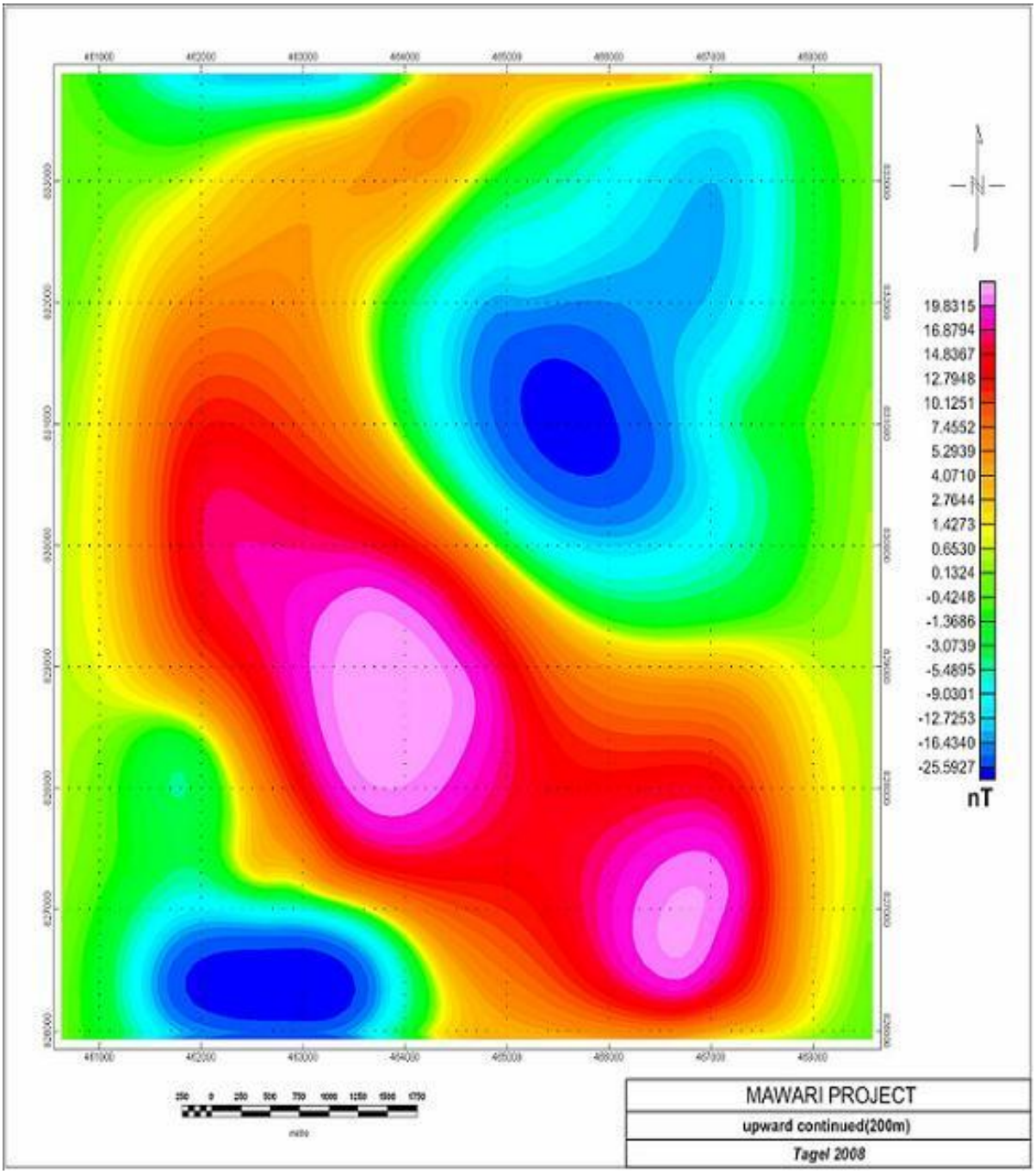

Figure 4.17 Upward continued (up to 200m) map of the study area.

4.4 Modeled Sections (Gravity and Magnetic Inverse Modeling)

The inverse modeling is done using GMSYS 3.05G software which is the product of GEOSOFT. For this study three lines were prepared but only the first and last lines were used for modeling purpose. Both the lines are nearer to the lakes, line-1 nearer to Lake Langano and line-3 is closer to Lake Shala. The bouguer anomaly values and the corrected total magnetic field values were used to produce the two modeled sections by choosing the option to perform both the potential fields simultaneously.

The observed gravity and magnetic profiles are composed of stations; locations where gravity and / or magnetic measurements have been made and where the model response will be calculated. Gravity stations generally lie on the topography of the model if they are land-based gravity readings. Magnetic stations may be on land or at some altitude, in the case of an aeromagnetic survey. But for this study both methods were conducted on land.

When GM-SYS calculates the potential response of a model, it will calculate and plot the total response of the model at each station. The observed response at each station over the cross section will also be plotted. This will allow oneself to model a cross section to match existing data.

Figure 4.18 and Figure 4.19 presented the two-modeled section, which were generated with the GM-SYS software. The modeling software calculates and displays the potential field responses from a user-defined geologic class selection and based on the least-squares best fit allows inversion. The best fit of the calculated potential fields (gravity and magnetic) values were generated from the proposed model section with the respective observed values while adjusting systematically varying the size, shape, density and susceptibility of the sections. Both the modeled sections were prepared based on some prior information on the general stratigraphy of the study area (Meseret TekleMariam, 1996). The other prior information used was the result of the EAGLE (Ethiopia Afar Geoscientific Lithologic Experiment) project. For this study the results of shot point 21-23 were considered to approximate the layer depth as well as the density values. In addition to the above, the ranges of density values for the rift system were considered from the work of Girma Woldetinsae (2005).

4.4.1 Modeled Section along Line-1

This modeled section is located between the geographic coordinates 463944E, 833209N and 466206E, 831042N and subdivided in to two parts: the first part shows up to a depth of 1260m from the surface and the second goes up to 8600m. This traverse has a length of about 3.12 km and NW-SE orientation. The station separation of the magnetic data was about 50m where as for gravity data 100m was used. Figure 4.18 A, shows the part of the modeled section which covers the upper layers having a total thickness of about

1260m from the ground surface. This section shows the overburden layer of the study area with different density values and the presence of geologic structures.

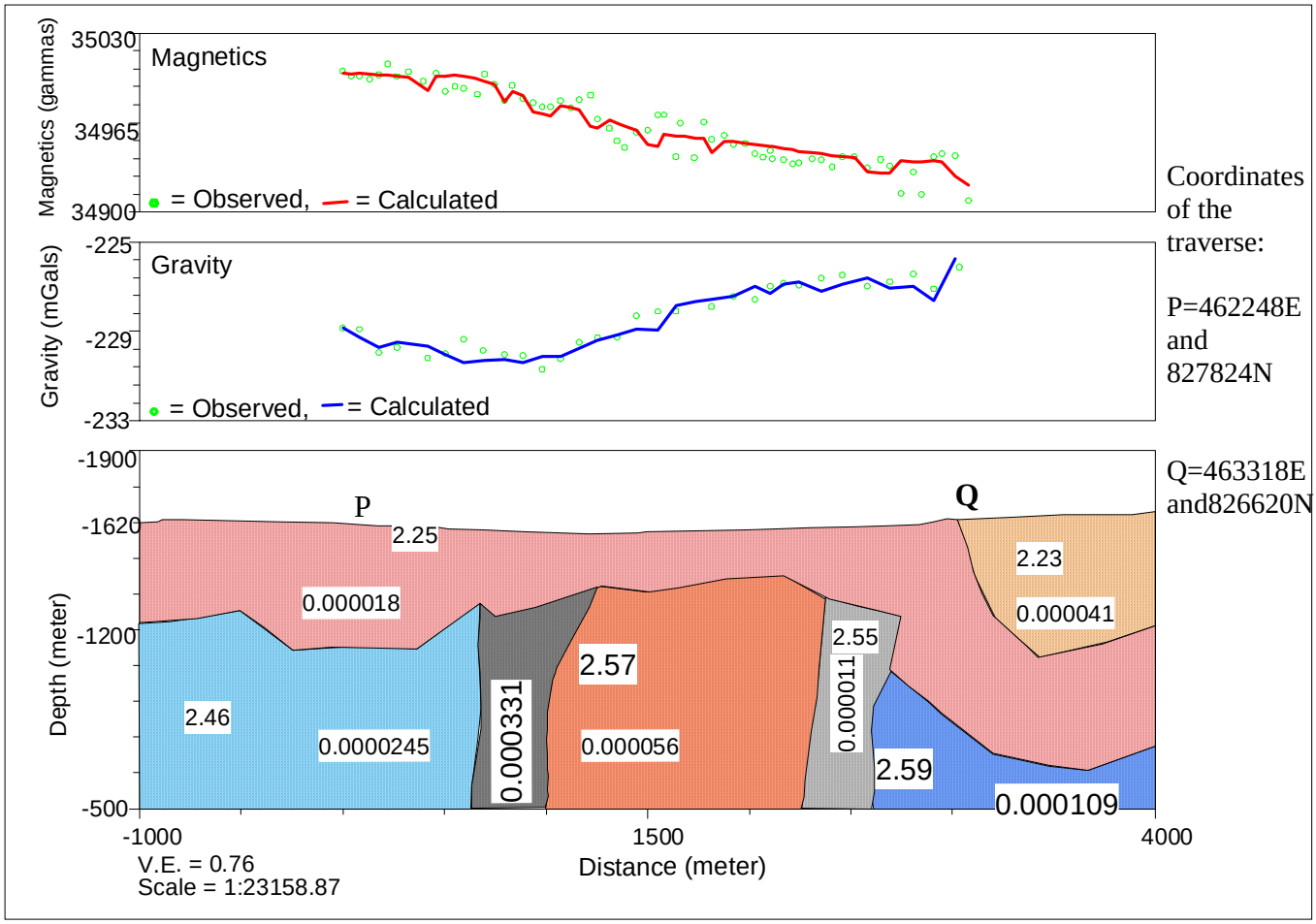

Figure 4.18 A: Modeled section along line 1 up to 1260 m from the ground surface.

Figure 4.18 B, below, shows the gravity and magnetic response of the probably geological formation of the study area along line 1.This figure shows a general increment on the gravity profile, which is the result of lateral density variations from NW to wards SE of the profile. The layers also show high density values when we go down ward which is the indication of the presence of relatively denser volcanic materials.

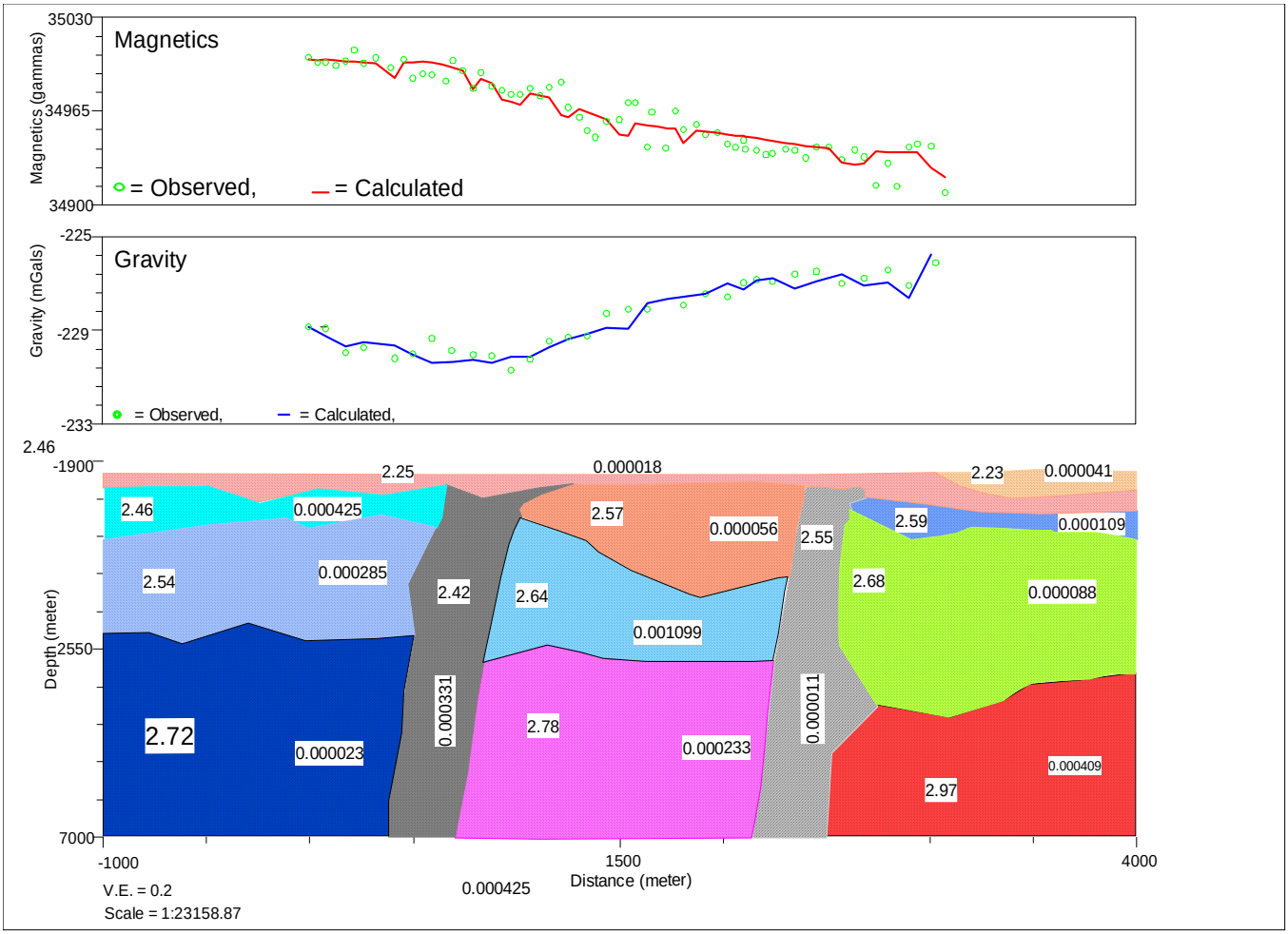

Figure 4.18 B: Modeled section along line 1 up to 8.76Km from the ground surface.

4.4.2 Modeled Section along Line-3

The traverse is located between the geographic coordinates 462248E, 827824N, and 463318E, 826630N. This traverse has a length of about 1.6 km and NW-SE orientation. The station separation of the magnetic data was about 50m where as for gravity data 100m was used. Figure 4.19 A, shows the part of the modeled section which covers the upper layers having a total thickness of about 1260m from the ground surface. This section shows the overburden layer of the study area with different density values and the presence of geologic structure.

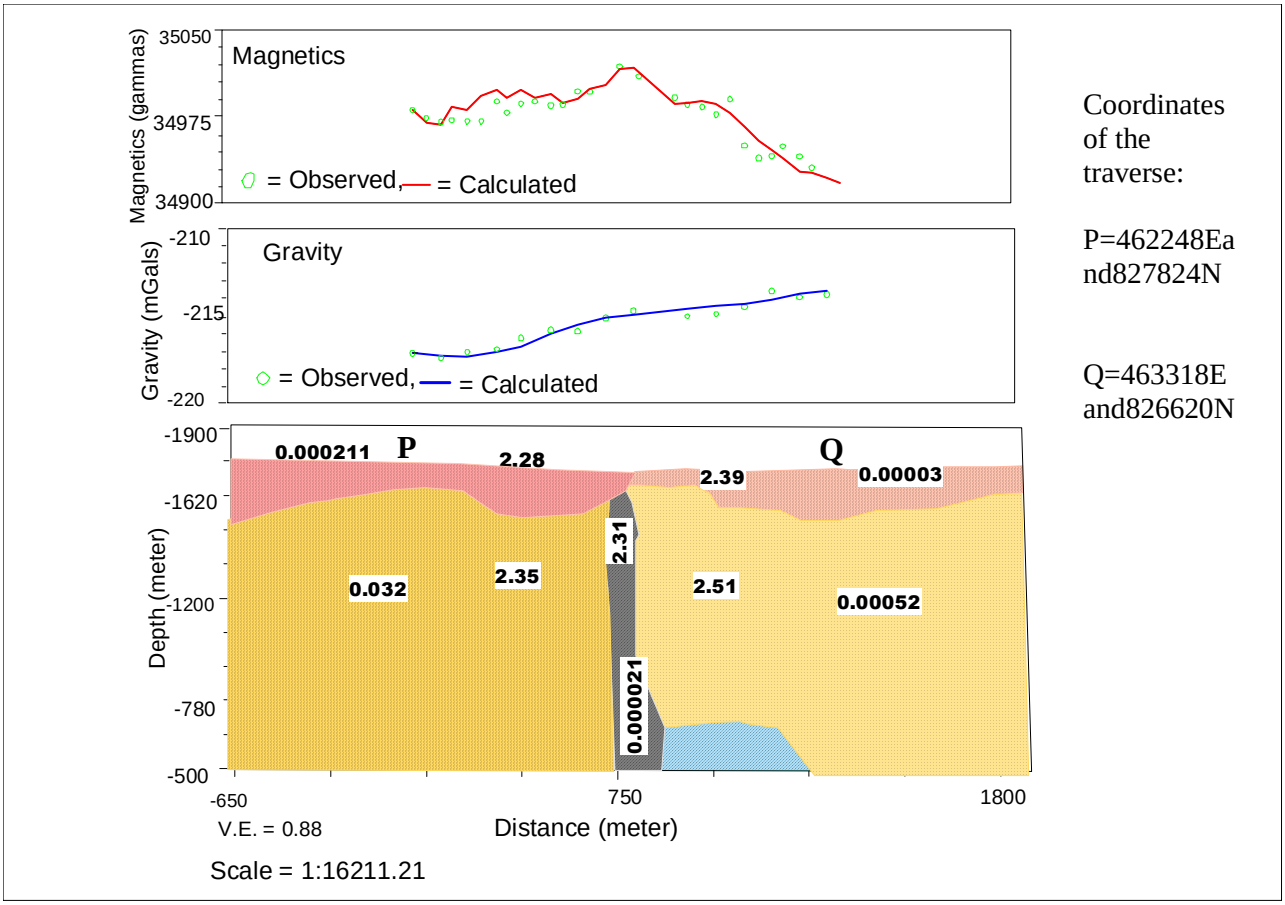

Figure 4.19 A: Modeled section along line 3 up to 1260 m from the ground surface.

.

The top two layers are believed to be consisting of different rock units such as lake sediment, ignimbrite, rhyolite and others which could be found being mixed with one another.

Figure 4.19 B, below, shows the gravity and magnetic response of the probably geological formation of the study area along line 3. We can see from this figure that there is a general increment on the gravity profile, which is the result of lateral density increment from NW to wards SE of the profile. The layers also show high density values when we go down ward which is the indication of the presence of relatively denser volcanic materials.

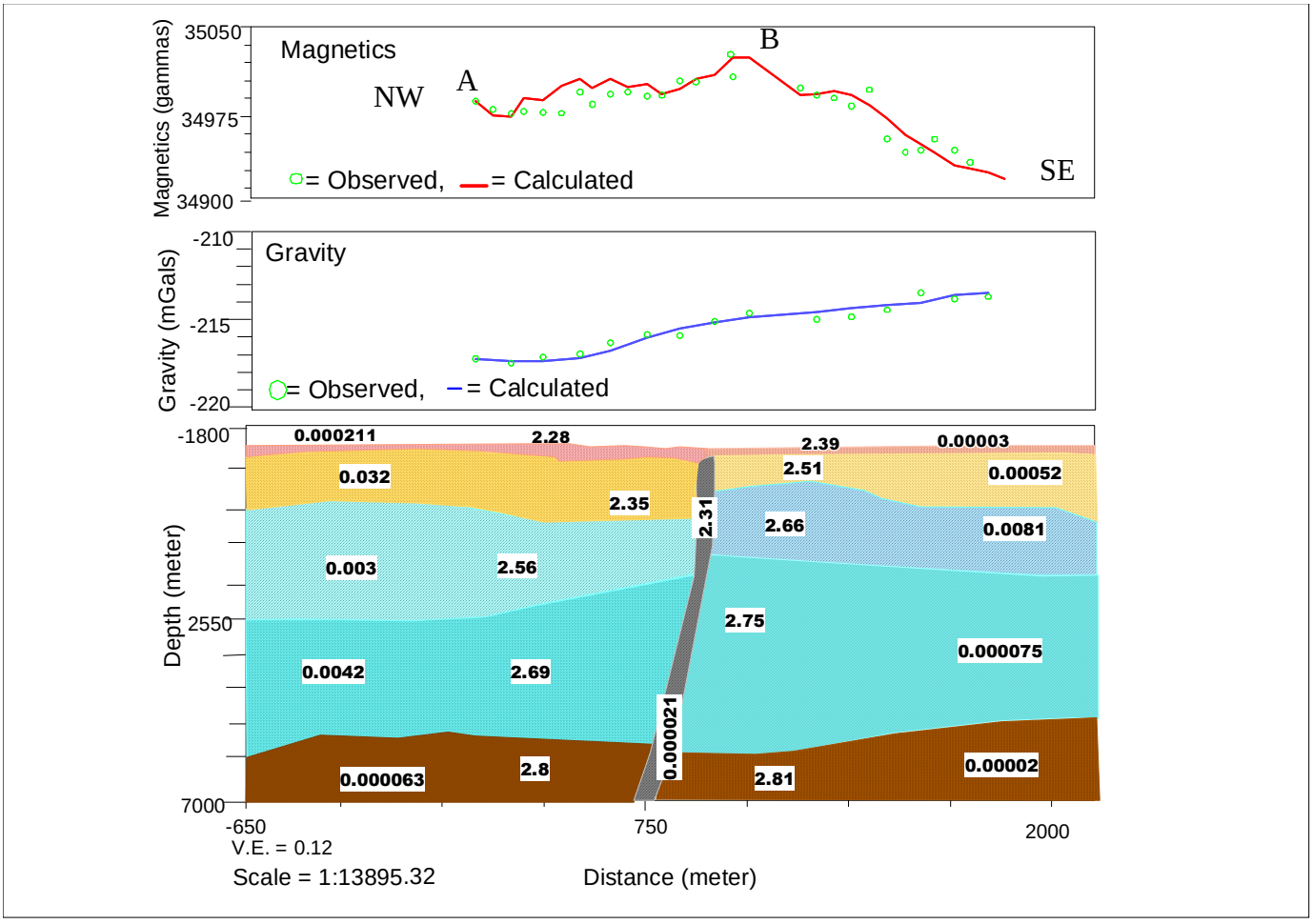

Figure 4.19 B: Modeled section along line 3 up to 8.76Km from the ground surface.

The vertical structure that divides the profile in to the left and the right part has density of 2.31 g/cc . This structure shows relatively lower density as well as susceptibility. Due to its lower density value relative to its surrounding, this structure may play very important role in conduit ground water at its top portion.

The total magnetic profile shows a steeply increasing of the total magnetic field starting from point A towards point B. Where as, from point B towards point C the total magnetic field decreases. These variations could be the result of the total effect of relatively higher susceptibilities values found at the right side layers compared to those layers found to the right side.

CHAPTER FIVE

DISCUSSION, CONCLUSION AND RECOMMENDATIONS

5.1 DISCUSSION

The objectives of this study were to map the presence of possible structures that may connect lakes Langano and Shala as well as to assess the ground water potential between the two lakes. Here we have conducted the three basic geophysical methods of prospecting namely: the electrical resistivity, the magnetic and the gravity methods, which are believed to be appropriate for the determination of the objectives of the study.

Previous geological and hydrological studies suggest the possibility of groundwater flow from Lake Langano to Lake Shala. These results are the outcome of the research conducted in the analysis of the water balance of the two lakes and geological and geophysical investigations which were carried out in the areas between the lakes to determine the existence of subsurface geological structures responsible for this fluid motion (Tenalem Ayenew, 1998).

This study is an additional work aimed at the study to map for the presence of such subsurface structures that could act as conduits for the flow of ground water between the two major lakes in the Main Ethiopian Rift, i.e. the Lake Langano Shala. Electrical, Magnetic and gravity methods of exploration were used in the study and a total of about 205 data points were collected on three survey traverses conveniently selected to lie in the areas between the two lakes. The result of this study were interpreted both qualitatively and quantitatively and presented on the preceding chapters.

From the results of electrical resistivity, we can understand that the study area is very affected by the presence of ignimbrite which is the dominant rock unit that forms from the highly resistive fresh ignimbrite to a low resistive and fractured ignimbrite which is inferred to be very good for conduiting and accumulating groundwater in the study area. The geoelectric sections show the

variations in the resistivity values along line 2 and line 3 which are inferred to be some kinds of contacts or structures that may help for the movement of groundwater.

The results of the potential methods were interpreted both qualitatively and quantitatively. The qualitative interpretation of the free-air anomaly map with the elevation map showed positive correlation. This correlation between the two maps, were taken as to show the overall accuracy of the survey. The long wavelength contour features and the relatively negative values in the Bouguer anomaly map and the magnetic anomaly map were interpreted to be due to deep seated geological formations, which are overlain by lower density formations.

Further, the quantitative interpretation from the 2D modeled sections which were generated using the GM-SYS modeling software on two of the profiles (Line 1 and Line 3) resulted in determining the physical properties, relative orientation and depth of different geological structures. From the result obtained in the evaluation of the lateral variation of density and susceptibility of the modeled sections, the presence of somehow faulted structures

The modeled section along Line-1 reveals the presence of relatively weak formations bounded by denser subsurface formations on either end off the traverse. This state of the subsurface is believed to be a result of tensional stress in the Rift system that opens up areas to be later filled by lighter alluvial deposits in the middle section. On the other hand modeled section of Line 3, a narrow vertical structure of relatively varying density and magnetic response is obtained.

5.2 CONCLUSION

Three of the geophysical prospecting methods namely; the electrical resistivity, the gravity and the magnetic methods were employed to fulfill the proposed objectives of the study. Based on the results obtained and the interpretations made, the following conclusions have been forwarded:

1. The apparent resistivity pseudo sections and the true resistivity geoelectric sections show the presence of shallow low resistivity horizons which are results of groundwater saturation.

2. The low resistivity and large thickness of these horizons is an indicator of high groundwater potential in the study area

3. The lower resistivity zones of the geoelectric sections possibly show the existence of groundwater movement between the two lakes forced by pressure head difference between the lakes.

4. The low bouguer anomaly in the study area may indicate a shallow origin that could be due to low density material of recent lake sediments.

5. The magnetic and gravity data analysis results in the form of modeled sections show the presence of structures on survey line 1 and line 3.

6. These structures are aligned in the general direction of rift (Southeast- Northwest direction)

7. The possible hydraulic link between the two lakes is expected to occur through the shallow low density horizons mapped on the traverses.

5.3 RECOMMENDATION

The ambiguity in the interpretation of a geophysical data arises due to the possibility of the same anomalous feature to be generated by a number different geological formation, which may be characterized by different physical appearance and physical property.

Based on the interpretations of the study, the following recommendations are forwarded to be implemented for ascertaining further the presence of subsurface geological structures of interest in the area of this study.

1. Electrical methods of prospecting, especially the electrical profiling/electrical imaging along one of the traverses to verify and validate the results of this work.
2. Seismic refraction survey, applied on limited but promising locations between the two lakes, to more precisely map the structures and also determine parameters such as densities of individual layers, depth to contacts, etc.

3. Further, geochemical investigations using hydrochemical and isotopic studies to correlate the water of the two lakes as regard to their origin and their interrelationships are also essential. .

References

Baker, B.H, Mohr, P.A. and Williams, L.A.J., (1972): Geology of the Rift System of Africa. *Geol.Soc. Am.,* Spec. paper, 136-67.

Boccaletti, M., Getaneh, A. and Torforici, L. (1992): The Main Ethiopian Rift: an example of oblique rifiting, *Ann. Tectonicae*, **6**,20-25

Di Paola, G.M., (1972): The Ethiopian Rift Valley (between $7^0$00' and 8^0 40'lat.North).
Bull. Volcanol, 36:517-560

Gidey, W., et al.1990. Geology , Geochronology and rift basin development in the central sector of the Main Ethiopian Rift. Bull. Geol.soc.America, Vol.102, 439-458

Girma Woldetinsae 2005. The Lithosphere of the East Africa Rift and Plateau (Afar-Ethiopia-Turkana): Insights from Integrated 3-D Density Modeling. Christian Alberchts University, Kiel, Germany. Pp 69

Harbie Hussen 2001.Gravity Survey of the Shala Caldera and Its Environs for the Exploration of Geothermal Energy. MSc. Thesis. Addis Ababa University

Jean-Jacques Tiercelin, Caroline Le Turdu and Francoise Gasse, 1997. International Symposium ''Flood Basalts, Rifting and Paleoclimates in the Ethiopian Rift and Afar Depression'' Addis Ababa, Ethiopia February 3-14, 1997

Kazmin, V. and Habitemichael Berhe, S. 1978. Geology and development of the Nazareth area. Ethiopian Institute of Geological Survey.

Kelley, S., 1999. Temporal and Geochemical characteristics of Tertiary volcanic rocks and tectonic history in the southern MER and the adjacent volcanic field. Acta. Vul. Vol II(1)99-119

Koefoed, O., (1970): A fast method of determining the layer distribution from the kernel function in geoelectrical sounding geophy.Prospecting.18:564-570

Meseret TekileMariam, 1996. Water rock interaction process in the aluto-Langano geothermal field, Ethiopia. Pisa, Italy. Pp 20-24

Milton B. Dorbin and Carl H. Savit , 1988. Introduction to Geophysical Prospecting. McGraw Hill Inc. Singapore

Mohr, P.A., (1967): The Ethiopian Rift system: ***Bull Geophyical observatory of Addis Ababa,*** **5**, 33-62.

Mohr, P.A., (1967a). The Ethiopian Rift System**:** *Bull. Geophysical Obs*. Addis Ababa, no.11, pp.1-65.

Mohr, P.A., (1971): The Geology of Ethiopia. Addis Ababa, Ethiopia. Addis Ababa University Press,

Mohr, P.A., (1971b): Outline of tectonics of Ethiopia, UNESCO, Tectonics of Africa, pp 445-458.

Mohr, P.A., (1667c): Major volcano-tectonic lineament in the Ethiopian Rift System, *Nature*, **213**, 664-665.

Mohr, P.A, Mitchell J.G., and Raynolds, R.G.H. 1980. Quaternary Volcanism and Faulting at O'a Caldera, Central Ethiopian Rift. Bull. Volcanol. , 43-1,173-189

Morley, C.K. 1999. Tectonic Evolution of the East African Rift System and its modifying influence of magmatism: A review. Acta vol.II(1) 1-19

Parasnis, D.S, (1962): Principles of Applied Geophysics (3rd edition). Chapman and Hall, London, pp98-121.

Robinson, Edwin S. 1988. Basic Exploration Geophysics. John Willey and Sons, Inc. USA

Telford, W.M., Sheriff, R.E., and Geldart, L.P., (1990). Applied Geophysics, Second ed., Cambridge, Cambridge University Press.

Tesfaye chernet 1982. Hydrogeology of the lakes region, Ethiopia (Lakes Ziway, Langano, Abiyata, Shalla and Awassa). Ministry of Mines and Energy, Ethiopian Institute of Geological Surverys,Addis Ababa , Ethiopia

Tenalem Ayenew, 1998. The hydrological system of the Lake District Basin, Central Main Ethiopian Rift. Published PhD. Thesis. ICT publication No 64, Enschede, The Netherlands. Pp 37-57

Tibebu Ayele 2001. Geophysical Studies In the Aluto Geothermal Area. MSc. Thesis. Addis Ababa University

WoldeGabriel, G., Aronson, J.L. and Walter, R.C (1990): Geology, Geochronology and Rift Basin Development in the central sector of the Main Ethiopian Rift. *Geological Society of* **Mohr, P.A., (1962a):** The Geology of Ethiopia .University collage press, Ethiopia *American Bulletin*, **102**, 439-458.

WoldeGabriel, G. 1987. Volcanotectonic history of the central sector of the Main Ethiopian Rift. PhD. thesis, Case Western Reserve Univ. , Cleveland, Ohio 410 pp.

WoldeGabriel, G., Aronson, J.L. and Walter, R.C (1990): Geology, Geochronology and Rift Basin Development in the central sector of the Main Ethiopian Rift. *Geological Society of American Bulletin*, **102**, 439-458.

Yemane, T.G., WoldeGebriel, G., Tesfaye, S., Derhe, S.M, Durary, S., Ebinger, C., Kelley, S., 1999. Temporal and Geochemical characterstics of Tertiary volcanic rocks and tectonic history in the southern MER and the adjacent volcanic field. Acta. Vul. Vol II(1) 99-119

Declaration

I, the undersigned, declare that this thesis is my original work, has not been presented for degrees in any other University and all Sources of material used for the thesis have been duly acknowledged.

Name: Tagel Assefa Dendi

Siginature: _____

Date: _____

This thesis has been submitted for examination with my approval as a University advisor

_____

Dr. Tigistu Haile.